Exploiting *Pseudomonas syringae* Type 3 secretion to study effector contribution to disease in spinach

Melanie Mendel[1,2], Xander C. L. Zuijdgeest[1,3], Femke van den Berg[1], Leroy van der Meer[1], Joyce Elberse[2], Petros Skiadas[4], Michael F Seidl[4], Guido Van den Ackerveken[2], Ronnie de Jonge[1,5*]

[1] Plant-Microbe Interactions, Department of Biology, Faculty of Science, Utrecht University, 3584 CH, Utrecht, The Netherlands

[2] Translational Plant Biology, Department of Biology, Faculty of Science, Utrecht University, 3584 CH, Utrecht, The Netherlands

[3] Current address: Centre for Plant Molecular Biology (ZMBP), University of Tübingen, 72076 Tübingen, Germany

[4] Theoretical Biology and Bioinformatics, Department of Biology, Faculty of Science, 3584 CH, Utrecht, The Netherlands

[5]AI Technology For Life, Department of Information and Computing Sciences, Science for Life, Utrecht University, 3584 CC, Utrecht, The Netherlands

* Correspondent author: Ronnie de Jonge, r.dejonge@uu.nl

Keywords: spinach, *Pseudomonas syringae*, effectors, effector screening, plant immunity

Funding: TopSector TKI Tuinbouw & Uitgangsmaterialen Grant Number: LWV19284, Enza Zaden Research & Development B.V. (NL), Pop Vriend Seeds (subsidiary of KWS Vegetables BV) (NL), Rijk Zwaan Breeding B.V. (NL), and Syngenta (NL).

21 Abstract

22 Intensive spinach cultivation creates favourable conditions for the emergence and rapid evolution of
23 pathogens, leading to substantial economic losses. Research on host-pathogen interactions in leafy
24 greens would benefit from advanced biotechnological tools, however absence of such tools in spinach
25 hampers our understanding of spinach immunity. Here, we explored the potential of Type III Secretion
26 System (T3SS)-mediated effector delivery to study pathogen effector activity in spinach. We identified
27 the *Pseudomonas syringae* pv. *tomato* DC3000 (DC3000) polymutant D36E, which lacks 36 known T3SS
28 effectors (T3Es), as a promising T3SS-dependent effector delivery system for spinach. Unlike DC3000,
29 which causes necrotic symptoms on spinach and reaches high bacterial titres, D36E did not proliferate
30 and caused no visible symptoms. Using D36E, we screened 28 DC3000 T3Es in spinach, assessing
31 symptom development, bacterial proliferation, and reactive oxygen species (ROS) bursts as a proxy for
32 early immune responses. AvrE1 and HopM1 emerged as key determinants of DC3000-like infection,
33 inducing water-soaked lesions, while HopAD1 strongly suppressed ROS production. Our findings
34 establish the D36E-based effector delivery system as a powerful tool for high-throughput effector
35 studies in spinach. It bridges the gap between genomics-based effector predictions and experimental
36 validation, paving the way for knowledge-driven resistance breeding in non-model crops like spinach.

37

38 ## Introduction

39 As consumers increasingly opt for healthier dietary alternatives, spinach has seen a remarkable rise in
40 its economic significance (Kandel et al., 2019). To meet the increasing demand, growers cultivate spinach
41 at high density, providing favourable conditions for the outbreak and rapid evolution of pathogens. The
42 oomycete *Peronospora effusa* (*P. effusa*) poses a major threat to global spinach production. It infects
43 spinach leaves, and causes downy mildew disease, rendering the crop unsellable and resulting in
44 substantial economic losses (Ribera et al., 2020). Other agronomically relevant spinach pathogens
45 include the oomycetes *Albugo occidentalis, Pythium spp.*, the fungus *Colletotrichum dematium,* and
46 viruses like the cucumber mosaic virus (Kandel et al., 2019; Ribera et al., 2020). To mitigate the impact
47 of these pathogens on spinach production, targeted improvement of crop resistance is crucial. However,
48 unlike other leafy greens such as lettuce, spinach lacks biotechnological tools to study its immunity,
49 limiting our ability to identify and develop novel disease resistance traits efficiently.

50 Our understanding of the spinach immune system remains limited and is primarily based on comparative
51 genome analysis and transcriptomics of disease resistance. For example, a comparison of *P. effusa*-
52 susceptible and *P. effusa*-resistant spinach cultivars transcriptomes showed that defence-related genes
53 like *PR-1* and diverse types of immune receptor genes, including the receptor-like kinase *FERONIA*, are
54 upregulated in resistant spinach cultivars (Kandel et al., 2020; Clark et al., 2024). *FERONIA* is
55 hypothesized to play a role in plant immunity, including the downstream production of reactive oxygen
56 species (ROS), a key component of plant immunity (Cheung, 2024). Immune receptors such as the
57 receptor-like kinases (RLKs) and nucleotide-binding leucine-rich repeat receptors (NLRs) are involved
58 with a variety of immune responses including, programmed cell death also known as the hypersensitive
59 response (HR), preventing the spread of pathogens (Jones and Dangl, 2006; Ngou et al., 2022). The

60 spinach genome encodes several hundred NLRs, of which the role in pathogen detection is largely
61 unknown (Xu et al., 2017; Hulse-Kemp et al., 2021).

62 Likewise, we know little about the molecular disease-related processes that are important during
63 spinach-pathogen interactions, including the activity and targets of pathogen effectors. Only recently,
64 genomic resources for spinach and its pathogens became available (Hulse-Kemp et al., 2021; Fletcher et
65 al., 2022, Skiadas et al., 2024). Nevertheless, no effector has been thus far identified to be recognized by
66 spinach (Cai et al., 2021). Identifying effectors and corresponding immune receptors would greatly
67 benefit future research and breeding efforts for disease-resistant spinach but requires high-throughput
68 methods to screen large number of putative effectors. To screen for effector recognition, typically,
69 *Agrobacterium*-mediated transient expression assays are used (Lu et al., 2016; Pelgrom et al., 2019).
70 Recent reports on improved *Agrobacterium*-mediated transient expression in spinach focused on fine-
71 tuning of individual protein expression levels but were not designed to detect immunity- or
72 pathogenicity-related phenotypes (Zhang et al., 2024). Alternatives approaches to deliver effector
73 candidates into plants include biolistic methods, nanoparticles, chemical transformations, fusion
74 peptides, and the bacterial Type 3 Secretion System (T3SS), however, to date, none of these have been
75 explored in spinach for effector research (Rustgi et al., 2022). Here, we evaluated the potential of the
76 T3SS as a method for studying pathogen effectors in spinach. The T3SS, a molecular syringe, is essential
77 for the delivery of bacterial effectors into the host cell (O'Malley and Anderson 2021). T3SS mutants
78 typically display reduced virulence, underscoring the importance of T3SS-delivered effectors (T3Es) in
79 establishing disease (Yuan and He 1996). Using the effectorless *Pseudomonas syringae* pv. *tomato*
80 DC3000 polymutant D36E, we here show that in the absence of T3Es, D36E survives in spinach leaves
81 while causing no detectable symptoms. To verify if D36E can deliver effectors in spinach, we

82 reintroduced 28 known DC3000 T3Es into D36E and evaluated theircontribution to symptom
83 development, bacterial proliferation, and ROS burst alterations, an early marker of plant immunity. We
84 demonstrate the effects of several of these effectors on these phenotypes in spinach, supporting
85 previous evidence that these effectors target conserved components of plant immunity and physiology.
86 OBJ

87 ## Results

88 ### Identification of *Pseudomonas* strain D36E as a candidate for T3SS-dependent effector delivery in
89 spinach

90 To study effectors in spinach, we first sought to identify a T3SS-encoding bacterial strain that is suited
91 for the delivery of effectors through the T3SS into spinach. As initial indicator of a bacterium's suitability
92 for T3SS-dependent effector delivery, we tested for the absence of visible changes at the infiltration site,
93 and the bacterium's ability to sustain a population when inoculated into spinach leaves (Figure 1). We
94 tested multiple *Pseudomonas* strains that were previously employed to deliver effectors in other hosts,
95 i.e.: 1) the Effector-to-Host-Analyser strain (EtHAn), a non-pathogenic *Pseudomonas fluorescence* (*Pf*-0)
96 strain that had been genetically engineered to express a T3SS and has been successfully employed in
97 multiple plants across several studies (Thomas et al., 2009; Krasileva et al., 2011; Upadhyaya et al., 2013);
98 2) the wildtype *Pseudomonas syringae* pv. *tomato* DC3000 (DC3000) strain, a natural pathogen of tomato
99 and that has been used to study effectors in other plants (Buell et al., 2003; Fabro et al., 2011); 3)
100 multiple DC3000 mutants with reduced effector arsenals, i.e., the DC3000$^{\Delta CEL}$(Δ*CEL*) mutant that lacks a
101 conserved effector locus, the nearly effectorless DC3000^{D28E} (D28E) polymutant, and the effectorless
102 polymutant DC3000^{D36E} (D36E) (Alfano et al., 2000; Cunnac et al., 2011; Wei et al., 2015); and 4) a
103 *Pseudomonas syringae* pv. *phaseolicola* (*Pph*) strainthat is a natural pathogen of bean and has displayed

104 promising results in preliminary work on spinach (Arnold et al., 2011). Lastly, we included a fourth
105 DC3000 mutant, the T3SS mutant DC3000$^{\Delta hrcC}$ (Δ*hrcC*) that cannot assemble a functional T3SS and is
106 therefore unable to deliver T3Es (Yuan and He, 1996).

107 We syringe-infiltrated the first true leaves of 2.5-3-week-old spinach with *Pseudomonas* bacteria at high
108 optical densities at 600 nm (OD_{600}) equal to 0.2, 0.4 and 0.6. We then visually assessed infiltration sites
109 between 6 days post inoculation (dpi) and 7 dpi, confirming that Δ*hrcC* and *Pph* did not cause visible
110 symptoms at the infiltration site. EtHAn, DC3000, and Δ*CEL* consistently caused strong necrotic
111 symptoms at all tested concentrations and D28E induced only mild chlorosis at the highest
112 concentrations, while D36E caused no visible symptoms (Figure 1A). To estimate the corresponding
113 bacterial populations in spinach, we next measured bacterial titres in spinach as colony-forming units
114 (CFUs) at 0 dpi and 2 dpi (Figure 1B). The Δ*hrcC* and D36E strains exhibited 1.5- to 2-fold reductions in
115 bacterial titres at 2 dpi compared to 0 dpi. *Pph*, like Δ*hrcC,* showed reduced bacterial titres between
116 0 dpi and 2 dpi at an OD_{600} of 0.2. However, at higher inoculum densities (OD_{600} of 0.4 and 0.6), *Pph*
117 maintained bacterial titres at 2 dpi close to 0 dpi levels, suggesting that native *Pph* effectors may
118 contribute to titre stabilization. EtHAn, DC3000 and Δ*CEL*, all of which exhibited necrotic symptoms,
119 proliferated in spinach between 0 dpi and 2 dpi, increasing titres around 1.5-2 orders of magnitude. In
120 contrast, D28E and D36E behaved like Δ*hrcC*, with titres 1-1.5 orders of magnitude lower at 2 dpi
121 compared to 0 dpi. To assess whether D36E sustains a population in spinach after 2 dpi, we further
122 monitored its titres in leaves over a period of five consecutive days (Figure S1). We observed that D36E
123 titres stabilized after 1 dpi, indicating that D36E can persist in spinach for at least five days without
124 eliciting visible plant responses (Figure S1). Since the effectorless D36E polymutant did not induce visible

125 alterations yet encodes a functional T3SS to deliver effectors, we concluded that this strain is suitable
126 for effector delivery into spinach.

127 ## AvrE1 and HopM1 are key contributors to visible DC3000-like disease symptoms in spinach

128 Since infiltration of wildtype DC3000 induced necrotic symptoms in spinach, whereas D36E did not
129 (Figure 1), we hypothesised that these symptoms result from the activity of specific DC3000 effectors.
130 To test this, we assessed D36E's suitability as an effector delivery system by individually reintroducing
131 28 DC3000 effectors into D36E, generating a library of D36E strains, each carrying a single effector. We
132 then evaluated the impact of these effectors on symptom development at infiltration sites and bacterial
133 titres in spinach.

134 To systematically describe and categorise visual symptoms in spinach, we used a semi-quantitative
135 scoring matrix ranging from 0 (no symptoms, D36E-like) to 4 (strong necrosis, DC3000-like). While
136 representative images illustrate these symptoms, considerable variation was observed (Figures 2, S2).
137 Among the 28 tested single-effector D36E strains, 18 did not induce consistent symptoms beyond those
138 of D36E. In contrast, 10 effectors triggered diverse visible symptoms. The clearest symptoms were seen
139 with *AvrE1* and *HopM1,* which caused strong necrosis in over 80% of infiltration sites (symptom score
140 >2), closely followed by *HopAM1*, which also produced symptoms similar to those caused by DC3000.
141 *HopF2* and *HopN1* also resulted in a disease-score >1 in at least 65% of infiltration sites, though with
142 variable frequency and severity. For example, *HopF2* predominantly induced chlorosis, with necrotic
143 lesions occurring in fewer than half of the infiltration sites. Infiltration of D36E carrying *AvrPtoB*, *HopAD1*,
144 *HopAO1*, *HopR1*, and *HopU1* significantly increased symptom frequency, though symptom scores >1
145 were inconsistent, appearing in only 27%-47% of infiltration sites.

146 ## *AvrE1*, *HopM1* and *HopU1* significantly affect bacterial proliferation in spinach

147 To assess whether D36E effector delivery can identify effectors that enhance bacterial proliferation, we
148 measured the contribution of 28 single effectors on early D36E growth in spinach (Figure 3A). Bacterial
149 titres at 2 dpi revealed three effectors that significantly affected D36E growth. Among them, AvrE1 and
150 HopM1 significantly increased D36E titres by a fold difference of $\log_{10}$ 2.3 and 1.3 respectively, whereas
151 HopU1 reduced them by a fold difference of $\log_{10}$ 0.9 (Figure 3B). The remaining D36E strains showed
152 no significant differences in titres compared to the D36E control, suggesting a limited impact on early
153 proliferation. Notably, while *HopN1*, *HopAM1*, and *HopF2* induced symptoms similar to those of DC3000,
154 they did not enhance D36E proliferation (Figures 2, 3B). Only *AvrE1* and *HopM1*, showed a correlation
155 between effector-driven necrosis and bacterial proliferation, suggesting that they actively manipulate
156 the host to create a beneficial niche.

157 ## Inoculum density influences effector-driven phenotypes in spinach

158 To further investigate the relationship between bacterial proliferation and necrotic symptoms, we
159 conducted infiltration experiments using 10-fold and 100-fold lower inoculum densities (OD_{600} equal to
160 0.04 and 0.004) for a subset of bacterial strains (Figures S3A-B). We focused on the control strains D36E
161 and DC3000, as well as D36E carrying two effectors with contrasting effects: *AvrE1*, which enhanced both
162 symptom development and bacterial proliferation, and *AvrPto*, which behaved similarly to the D36E
163 control. Additionally, we measured bacterial titres at 6 dpi, when visual symptoms were previously
164 assessed (Figure S3C).

165 Based on prior assays, we expected D36E and *AvrPto* populations to decline between 0 dpi and 2 dpi,
166 while DC3000 and *AvrE1* titres were anticipated to increase (Figures 2, 3), and as bacterial titres
167 remained stable up to 5 dpi (Figure S1), we expected similar trends at 6 dpi. Overall, bacterial titres

168 scaled proportionally with reduced inoculum densities, except for *AvrE1* at 100-fold dilution, which no
169 longer exhibited enhanced growth (Figure S3A). Interestingly, when diluted 10-fold, DC3000 exhibited a
170 greater increase in growth (two orders of magnitude) compared to the original OD_{600} of 0.4, which
171 showed less than a one-order-of-magnitude increase, suggesting that bacterial growth may plateau at
172 higher inoculum densities. Regardless of inoculum density, DC3000 consistently triggered strong
173 necrosis, whereas *AvrE1*-induced necrosis was markedly reduced at lower densities (Figure S3B). These
174 results indicate that assay outcomes can be dose-dependent, with a minimum inoculum density
175 potentially required to detect relevant phenotypes in spinach using the D36E effector delivery system.
176 At 6 dpi (OD_{600} equal to 0.4), titres of D36E and *AvrPto* were lower than at 2 dpi, whereas *AvrE1* titres
177 remained stable (Figure S3C). Notably, DC3000 titres significantly decreased between 2 dpi and 6 dpi
178 (Figure S3C), suggesting that bacteria in necrotic infiltration sites ultimately die.

179 ### *AvrE1*, *HopM1* and *HopAD1* reduce MAMP-induced ROS bursts in spinach

180 Reactive oxygen species (ROS) bursts are an early immune response in plants, acting as a defence against
181 plant pathogens (Ngou et al., 2022). Consequently, successful pathogens have evolved mechanisms to
182 suppress ROS bursts (Jwa and Hwang, 2017). To investigate the role of bacterial effectors in modulating
183 early immune responses in spinach, we adapted a ROS burst assay for D36E-based effector screening,
184 following established *Nicotiana benthamiana* methodologies (Johanndrees et al., 2022; Figure 4A).

185 First, we screened known ROS burst elicitors to identify the most potent triggers in spinach leaf discs.
186 We tested chitin (Sánchez-Vallet et al., 2015), the flg22 peptide (Mersmann et al., 2010), the nlp24
187 peptide from a downy mildew Nep1-like protein (Oome et al., 2014), heat-lysed *P. effusa race 1*
188 sporangia (Pe1 sporangia) (Klein et al., 2020; Skiadas et al., 2022), and a microbe-associated molecular
189 pattern (MAMP) extract from heat-lysed D36E cells (Wei et al., 2015) (Table S5). Among these, chitin,

190 the MAMP-extract, and Pe1 sporangia triggered significant ROS bursts, with the MAMP-extract inducing
191 the strongest response (Figure S4). Therefore, we selected the MAMP-extract as elicitor for subsequent
192 assays.

193 Next, we established controls for D36E-compatible ROS assay. We compared ROS production in spinach
194 leaf discs pre-infiltrated with either D36E or a mock solution (Figure S5). Pre-infiltration with D36E alone
195 (D36E/MQ) did not alter ROS levels compared to the mock control, whereas treatment with the MAMP-
196 extract after D36E infiltration (D36E/MAMPs) triggered a robust ROS burst. Based on these results, we
197 used D36E/MQ as the negative control and D36E/MAMPs as the positive control (Figure 4B). When we
198 tested DC3000 (OD_{600} equal to 0.4), we observed significant ROS suppression compared to the D36E/MQ
199 negative control, which we attributed to effector-mediated suppression (Figure S6).

200 Finally, we screened the D36E single-effector library to identify effectors that suppress the MAMP-
201 extract-induced ROS burst in spinach (Figure 4C). Among the 28 tested effectors, *AvrE1*, *HopAD1*, and
202 *HopM1* significantly reduced ROS production. Notably, *HopAD1* suppressed ROS bursts to levels
203 comparable to the D36E/MQ negative control, even exceeding the suppression observed in DC3000-
204 infiltrated leaf discs. Most other effectors did not significantly alter ROS burst levels, indicating that the
205 ability to suppress early immune responses is limited to a specific subset of effectors.

206 ## Only AvrE1 and HopM1 largely restored DC3000-like characteristics on spinach

207 To identify similarities among individual DC3000 effectors across different assays in spinach, we
208 systematically compared phenotypic outcomes for each strain. To enable a direct comparison, we
209 standardized phenotypic responses using Z-scaling and applied hierarchical clustering (Figure 5). This
210 analysis revealed five distinct effector clusters (Clusters I–V), each characterized by a unique

211 combination of phenotypic patterns. Cluster I includes DC3000, *HopM1*, and *AvrE1*, confirming that
212 these two effectors can largely restore DC3000-like effects for the assessed phenotypes in spinach.
213 Cluster II consists of a single strain, *HopAD1*, which strongly suppressed the ROS burst while not affecting
214 proliferation and causing symptoms in 27% of infiltration spots (Figures 2-5), suggesting that ROS burst
215 suppression alone is insufficient to restore D36E proliferation. Cluster III includes *HopR1*, *HopAM1*,
216 *HopN1*, *HopF2* and *HopAO1* which induced significant symptoms, while not altering ROS bursts or
217 bacterial proliferation (Figures 2-5). Cluster IV comprised *AvrPtoB* and *HopU1*. These effectors reduced
218 bacterial proliferation (significantly for *HopU1*, Figure 3B), but had no impact on ROS production or
219 symptom development (Figures 2, 4C). Cluster V includes the remaining 18 effectors thatdid not show
220 any detectable phenotypic responses in our assays.

221 Consistent responses across cultivars supports broad applicability of type 3 effector delivery in spinach

222 Consistent phenotypic responses of the D36E-based delivery assay spinach cultivars are important for
223 future applications. We therefore assessed the robustness of our assay setup by testing multiple spinach
224 cultivars for their responses to key controls (D36E and DC3000) (Figure S7). We infiltrated five spinach
225 cultivars, i.e., Whale, Hydrus, NL3, NIL5 and NIL6 (OD_{600} equal to 0.4), and found that these all responded
226 similarly to the responses previously recorded in Viroflay, exhibiting necrosis with DC3000 infiltration
227 and no symptoms with D36E (Figure S7A). Similarly, bacterial proliferation patterns were consistent
228 across cultivars. Like Viroflay, D36E titres decreased between 0 dpi and 2 dpi, whereas DC3000 titres
229 increased in cultivars Whale, NIL3 and Caladonia (Figure S7B). To assess the suitability of our ROS assay
230 setup, we tested D36E/MQ (negative control), D36E/MAMPs (positive control) and DC3000/MAMPs
231 (suppressed control) on Whale and NIL3. The responses of these cultivars were comparable to those

232 observed in Viroflay (Figure S7C). Together, these findings indicate that our newly established spinach
233 type 3 delivery assays can be reliably applied across different spinach cultivars.

234 Discussion

235 To advance knowledge-driven resistance breeding in spinach functional studies on pathogen effectors
236 are of high importance. Here, we established an *in-planta* effector screening system using the
237 *Pseudomonas syringae* pv. *tomato* DC3000 polymutant D36E (D36E) as a protein delivery system. This
238 system allowed us to systematically assess the contribution of DC3000 effectors to disease susceptibility
239 and symptom development in spinach. Among the 28 bacterial effectors tested, we identified *AvrE1* and
240 *HopM1* as key drivers of the DC3000 phenotype, both promoting necrosis and bacterial proliferation,
241 while also suppressing the reactive oxygen species (ROS) burst. We also identified *HopAD1* as a potent
242 suppressor of ROS bursts, though its effect on bacterial fitness in spinach remained inconclusive.
243 Moreover, we found that expression of the effectors *HopAM1*, *HopAO1*, *HopF2*, *HopN1* and *HopR1*
244 contributed to symptom development without significantly affecting D36E proliferation. To our
245 knowledge, this represents the first report of a functional *in planta* effector screen in spinach,
246 establishing a foundation for future resistance studies.

247 AvrE1 and HopM1 drive bacterial virulence in spinach

248 A major challenge in interpreting our findings is the lack of a confirmed, recognized effector in spinach
249 to benchmark our observations. In the non-host plant *Nicotiana benthamiana,* AvrE1, HopM1 and
250 HopAD1 act as elicitors of effector-triggered immunity (ETI), inducing a characteristic response of
251 programmed cell death and restricted bacterial growth (Wei, Zhang et al. 2018). In spinach, we found
252 that *AvrE1* and *HopM1* induce necrosis similar to DC3000. Unlike observations in *N. benthamiana*,
253 necrosis in spinach was accompanied by increased bacterial titers compared to the negative control

254 D36E (Figures 2, 3). We initially attributed this to relatively high infiltration density. However, the
255 increase in bacterial titres between 0 dpi and 2 dpi persisted even at lower inoculum densities and at
256 later timepoints (Figures S3A, C). Therefore, we hypothesise that necrosis is the result of successful
257 bacterial infection rather than an active plant immune response.

258 Expression of *AvrE1* and *HopM1* in D36E resulted in comparable phenotypic outcomes in spinach (Figure
259 5). Functional redundancy among these two effectors was extensively described in model plants
260 including DC3000's natural host, tomato, but also in *N. benthamiana* and *Arabidopsis thaliana*
261 (*Arabidopsis*) (DebRoy et al., 2004; Badel et al., 2006; Cunnac et al., 2011). In DC3000, these effectors
262 are encoded alongside each other at the conserved effector locus (*CEL*) that is widely distributed among
263 plant-infecting bacteria of the genus *Pseudomonas* (Baltrus et al., 2011). Both effectors contribute to the
264 creation of an aqueous micro-environment on host plants, which is crucial for successful *Pseudomonas*
265 infection (Roussin-Léveillée et al., 2022). In spinach, we observe water-soaked lesions—symptomatic for
266 the establishment of an aqueous micro-environment—following inoculation with D36E bacteria carrying
267 *AvrE1* or *HopM1,* suggesting that their virulence targets are likely conserved in spinach.

268 On the molecular level, AvrE1 and HopM1 are distinct, belonging to different molecular families. AvrE1
269 belongs to a broadly conserved AvrE1/DspA/E/HopR1 superfamily of effectors (Kvitko et al., 2009;
270 Baltrus et al., 2011), while HopM1 is part of a less conserved effector family (Baltrus et al., 2011;
271 Jayaraman et al., 2020). In its superfamily, AvrE1 is the best characterized effector, recently
272 demonstrated to induce water-soaked lesions by forming a pore-forming beta barrel, thereby creating a
273 permeable membrane channel (Nomura et al., 2023). The pore-forming function appears not to be
274 shared by HopM1, which does not exhibit the distinct beta barrel structure or other prominent molecular

275 features (Nomura et al., 2023). In spinach, we observed that *AvrE1*, more than *HopM1*, could induce
276 DC3000-like symptoms by D36E (Figure 5A), possibly via its pore-forming function.

277 HopM1, like AvrE1, has been implicated in creating water-soaked lesions to enhance virulence in
278 *Arabidopsis* (Xin et al., 2016), which aligns with early phenotypes we observed in spinach. HopM1 was
279 shown to target the proteasome, a central point of regulation in plant immunity (Üstün et al., 2016).
280 HopM1 enhances AtMIN7 proteasome-dependent degradation consequently interfering with vesicle
281 transport in *Arabidopsis* (Nomura et al., 2006; Xin et al., 2016). In addition, HopM1 destabilises a range
282 of other proteins in a proteasome-dependent manner that include, e.g., 14-3-3 proteins like GRF8/TFT1
283 (Lozano-Durán et al., 2014). HopM1 was shown to reduce PAMP-triggered ROS bursts, similar to
284 chemical destabilisation of 14-3-3 proteins or a targeted silencing of GRF8/TFT1, suggesting that HopM1
285 targets 14-3-3 proteins to supress early immune responses like ROS bursts (Lozano-Durán et al., 2014).
286 We observed that infiltration of spinach leaves with D36E carrying *HopM1* significantly suppressed the
287 ROS burst, suggesting that the interference with 14-3-3 proteins might be conserved (Figure 4C).

288 ### HopAD1 suppresses the ROS burst but does not enhance bacterial growth

289 Infiltration of spinach leaves with D36E bacteria carrying *HopAD1* led to a strong suppression of the ROS
290 burst and the development of mild necrosis in 27% of infiltration spots (Figures 2, 4C). Compared to
291 AvrE1/HopM1, less information is available on HopAD1, as it was initially dismissed as a non-functional
292 effector (Chang et al., 2005). However, Wei and colleagues (2015) already described its potential to
293 suppress the ROS burst and trigger cell death in *N. benthamiana*. When the effector AvrPtoB is present,
294 like in the case of DC3000, HopAD1's immunogenic activities are masked in *N. benthamiana* leading to
295 the earlier dismissal of this effector (Wei et al., 2015). Since the nearly effector-less DC3000 mutant D28E
296 does not encode *AvrPtoB*, Wei and colleagues could successfully reveal its function (Wei et al., 2015).

297 While in spinach and in *N. benthamiana*, infiltration by D36E bacteria carrying *HopAD1* yielded strong
298 suppression of the ROS burst, only in *N. benthamiana*, infiltration at high titres also resulted in consistent
299 necrotic symptoms (Wei, Zhang et al. 2018, Figures 2, 4C). In *N. benthamiana*, cell death did not
300 necessarily lead to altered virulence, mimicking our findings in spinach (Wei, Zhang et al. 2018, Figures 2,
301 5). We propose that the suppression of the MAMP-induced ROS burst is a primary function of HopAD1,
302 which by itself appears to be insufficient to promote bacterial proliferation. Despite the identification of
303 HopAD1's immunogenic activity, the molecular mechanisms underlying its ability to suppress the ROS
304 burst while leaving bacterial proliferation unaffected in spinach remain elusive.

305 Effector redundancy and synergy in spinach

306 In nature, effectors often act synergistically and display redundancy. For instance, our findings reveal
307 that the Δ*CEL* mutant, characterized by the absence of *AvrE1*, *HopM1*, *HopN1* and *HopAA-1* (Alfano et
308 al., 2000; Wei and Collmer, 2018), induced robust visible symptoms and exhibited proliferation similar
309 to DC3000 at 2 dpi on spinach (Figure 1). This finding contrasts with our observations of single effectors,
310 wherein only *AvrE1* and *HopM1* could significantly enhance proliferation of D36E bacteria on spinach.
311 However, its DC3000-like virulence underscores the importance of synergistic effector action in nature.
312 The combined influence of the remaining effectors in the Δ*CEL* mutant appears to compensate for the
313 absence of *AvrE1* and *HopM1* in spinach, emphasizing the intricate synergies among effectors in shaping
314 the overall pathogenic response. Evidence for genetic interactions between DC3000 effectors has been
315 previously found in *N. benthamiana*, where HopAD1-dependent disease symptoms are suppressed by
316 AvrPtoB, and HopI1 suppressed cell death elicited by AvrE1, HopM1, HopR1, HopQ1-1 and HopAM1 (Wei
317 et al., 2015).

318 ## Conclusion

319 We present the first report of a functional *in planta* effector screen in spinach. In the future, the D36E
320 delivery system can be harnessed for characterising spinach pathogen effectors to identify those
321 recognised by the spinach immune system. Compared to native spinach pathogens such as the obligate
322 biotrophic oomycete *P. effusa*, the D36E effector delivery provides a simplified system to study effectors
323 in their native hosts. In contrast to *Agrobacterium*-mediated transient expression, our data suggest that
324 the D36E system performs similarly across spinach cultivars and does not require extensive fine-tuning
325 for biochemically distinct effectors like AvrE1, HopM1 or HopAD1 (Figures 2, S7) (Zhang et al., 2024).
326 Thus, we here introduce a novel approach for functional effector studies in spinach with potential for
327 high-throughput screening.

328

329 Figures

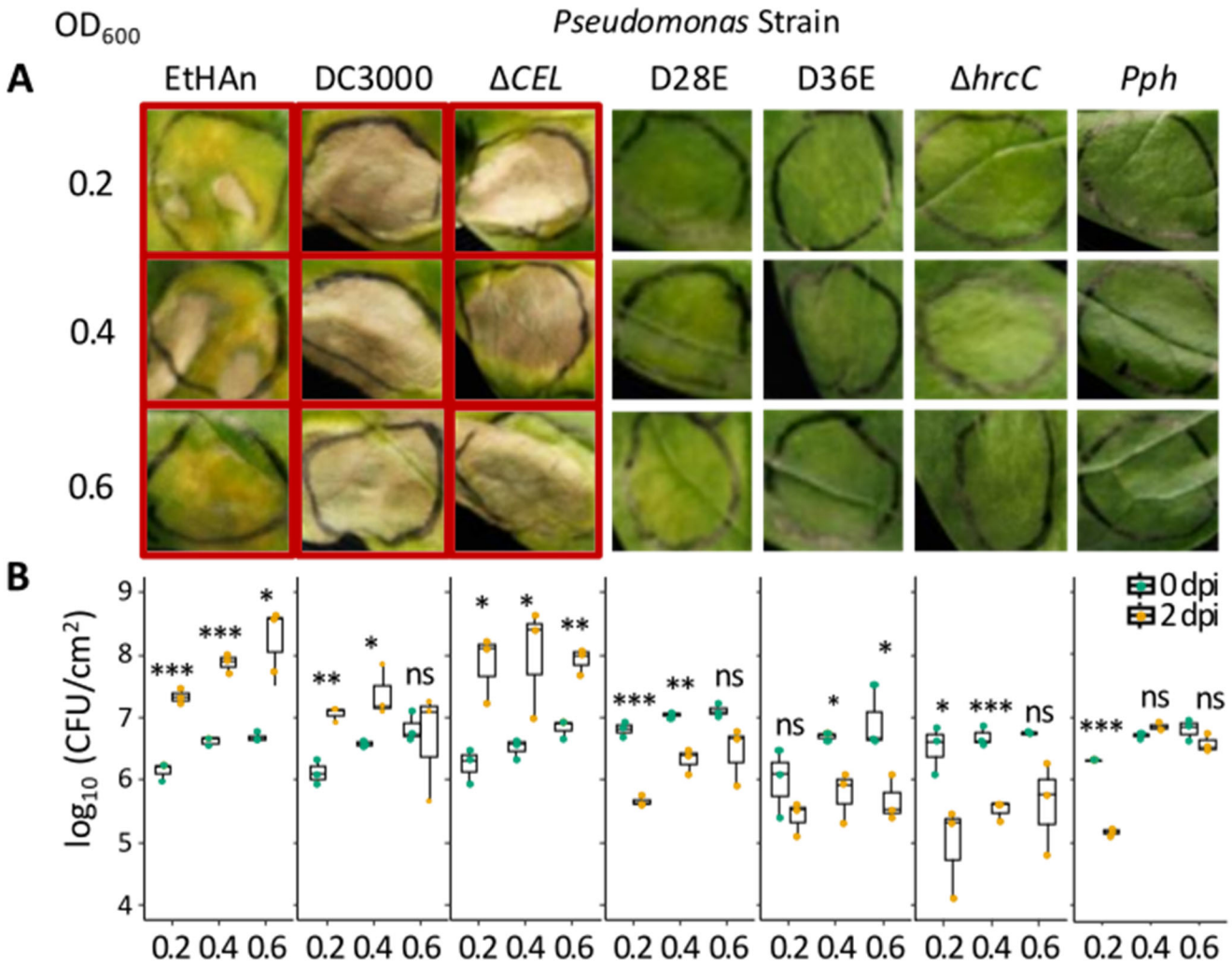

330

331 **Figure 1: *Pseudomonas syringae* pv. *tomato* DC3000 polymutant D36E is a suitable candidate for**
332 **effector screens in spinach. A)** Representative images of spinach leaves 6–7 days post infiltration (dpi)
333 with various *Pseudomonas* strains: the transgenic *Pseudomonas fluorescens* Pf-1 strain EtHAn (EtHAn),
334 *Pseudomonas syringae* pv. *tomato* DC3000 (DC3000), the DC3000 mutant strain Δ*CEL* (Δ*CEL*), the DC3000
335 effector polymutants D28E (D28E) and D36E (D36E), the DC3000 T3SS-mutant Δ*hrcC* (Δ*hrcC*) and the
336 bean pathogen *Pseudomonas syringae* pv. *phaseolicola* (*Pph*). Photographs were taken 67 days post
337 inoculation (dpi). Infiltration sites outlined in red highlight severe chlorosis and necrosis, particularly in
338 EtHAn-, DC3000-, and Δ*CEL*-infiltrated leaves. **B)** Bacterial proliferation quantified as $\log_{10}$ colony-
339 forming units (CFU) per square centimetre (cm^2) at 0 dpi (green; immediately after infiltration) and 2 dpi
340 (yellow). Infiltrations in **(A)** and **(B)** were performed on the first true leaves of 2.5-3-week-old spinach
341 plants at the indicated inoculum densities ($0D_{600}$ = 0.2, 0.4, and 0.6). Statistical significance between CFU
342 counts at 0 dpi and 2 dpi was determined using a two-tailed t-test (*** $p < 0.001$, ** $p < 0.01$, * $p < 0.05$;
343 $n = 3$ infiltration sites per treatment and timepoint).

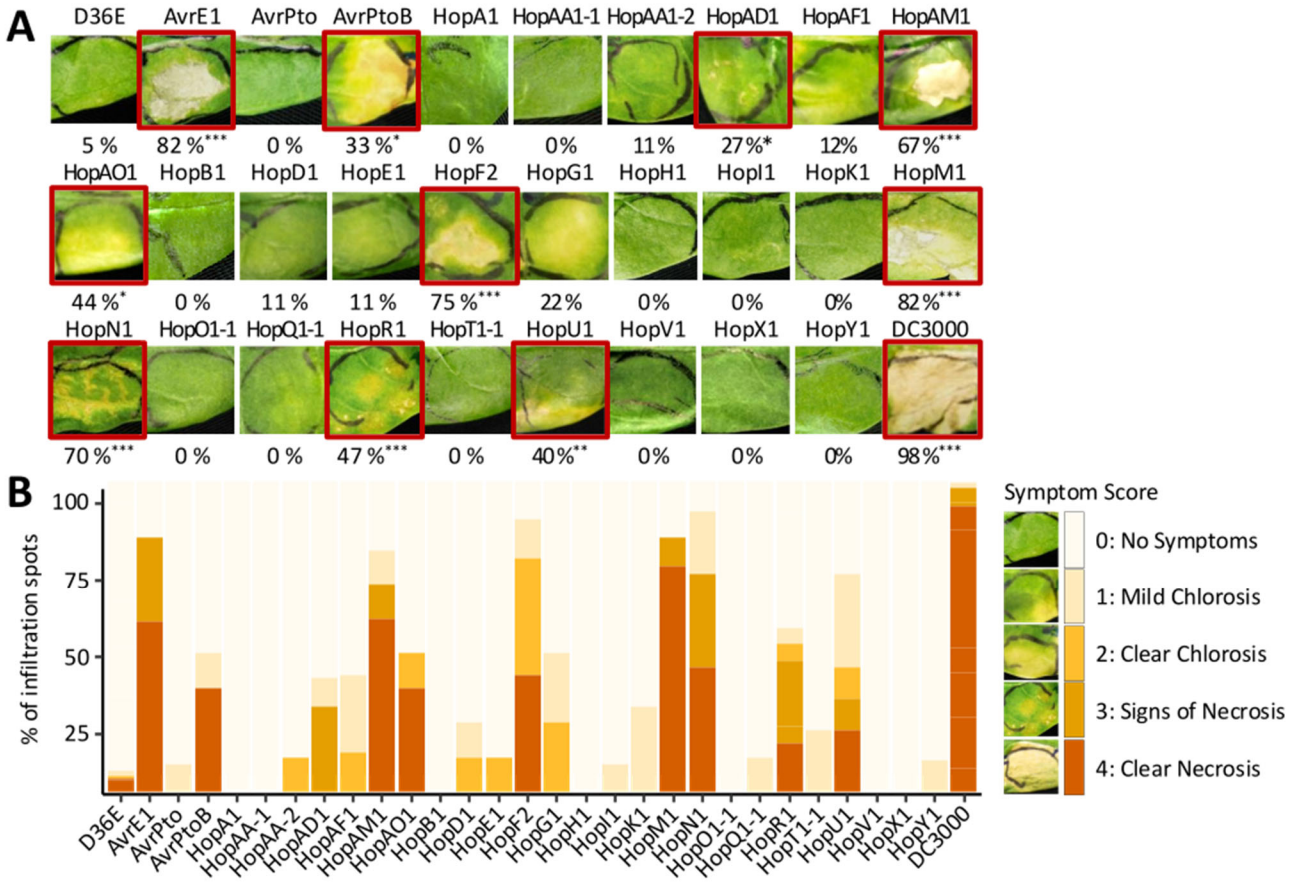

Figure 2: DC3000 effectors in D36E can reconstitute DC3000-like symptoms in spinach. A) Representative images of spinach leaves 6–7 days post-infiltration (dpi) with D36E, DC3000, and D36E strains expressing individual *P. syringae* DC3000 effectors. Symptoms were scored using a symptom scoring matrix ranging from 0 (no symptoms) to 4 (clear necrosis), with additional examples in Figure S2. The percentages below each image indicate the proportion of infiltration sites that developed visible symptoms (symptom score >1). D36E, serving as a negative control, induced symptoms at a negligible rate (5%), while DC3000 caused severe symptoms in most infiltration sites (98%). Effectors that significantly influenced symptom development ($p < 0.05$) are highlighted with a red border. Statistical significance was assessed using a Fisher's Exact test (*** $p < 0.001$, ** $p < 0.01$, * $p < 0.05$). **B)** Stacked bar graph showing the frequency distribution of symptom scores for each tested effector, using a colour gradient from light orange (mild chlorosis, symptom score 1) to dark orange (clear necrosis, symptom score 4). D36E bacteria expressing individual effectors, along with controls (D36E and DC3000), were infiltrated at $OD_{600} = 0.4$, with symptom development assessed at 6–7 dpi (n = 8–12 infiltration sites per treatment).

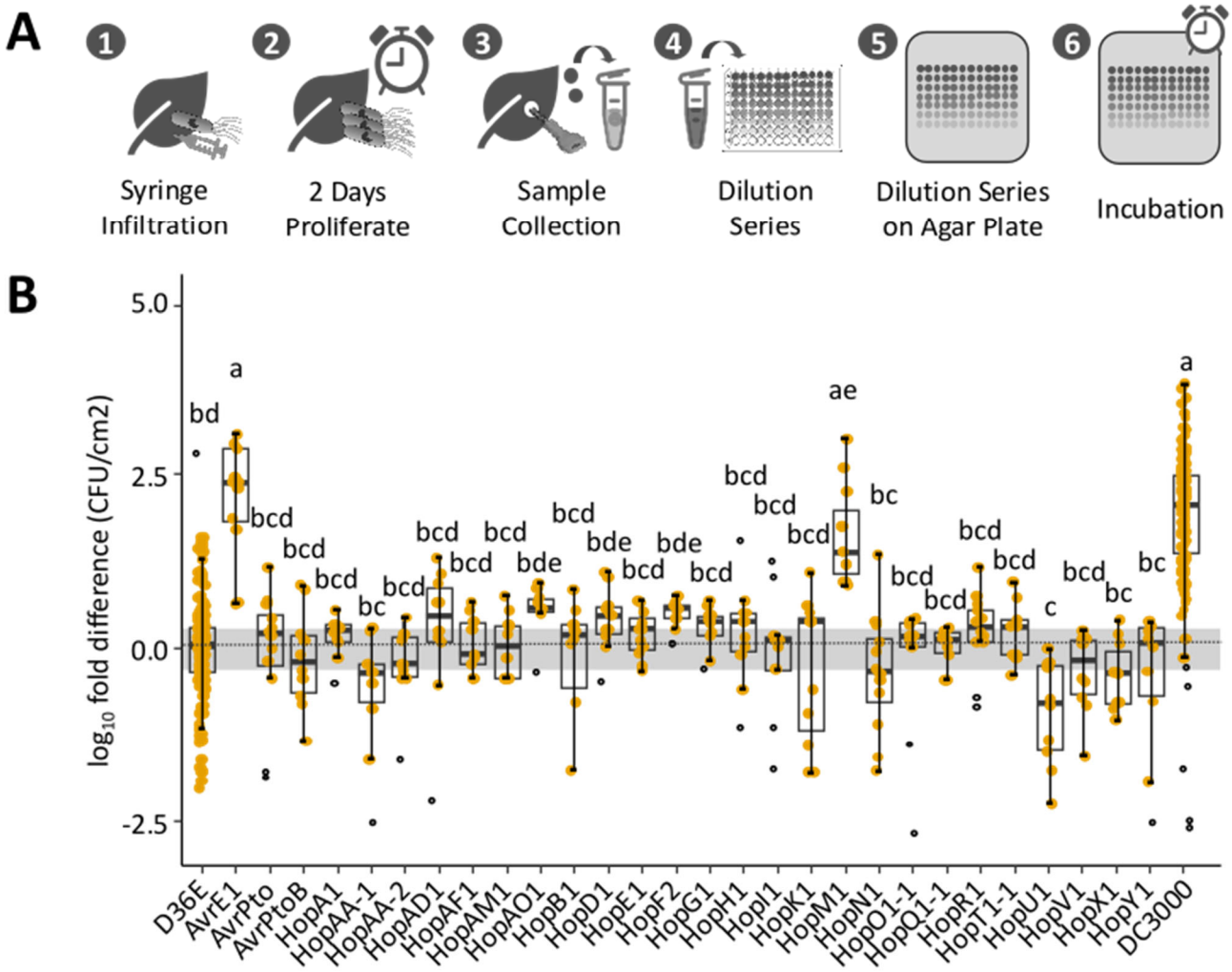

Figure 3: Expression of *AvrE1*, *HopM2*, and *HopU1* significantly alters D36E proliferation in spinach. **A)** Schematic overview of the bacterial quantification workflow. Spinach leaves were syringe-infiltrated with bacterial suspensions (Step 1), followed by a 2-day proliferation period (Step 2). Samples were then collected (Step 3) and subjected to serial dilution (Step 4) before plating on agar (Step 5) and incubating for colony counting (Step 6). **B)** Effect of individual DC3000 effectors on D36E proliferation, measured as the $\log_{10}$ fold difference in colony-forming units per square centimetre (CFU/cm^2) relative to the D36E negative control at 2 days post-infiltration (dpi). Each point represents an individual infiltration site, with measurements based on three pooled leaf discs (n = 8–12 per treatment). Statistical significance was determined using one-way ANOVA followed by Tukey's Honestly Significant Difference (HSD) test. Different letters above boxplots indicate statistically significant differences ($p < 0.05$).

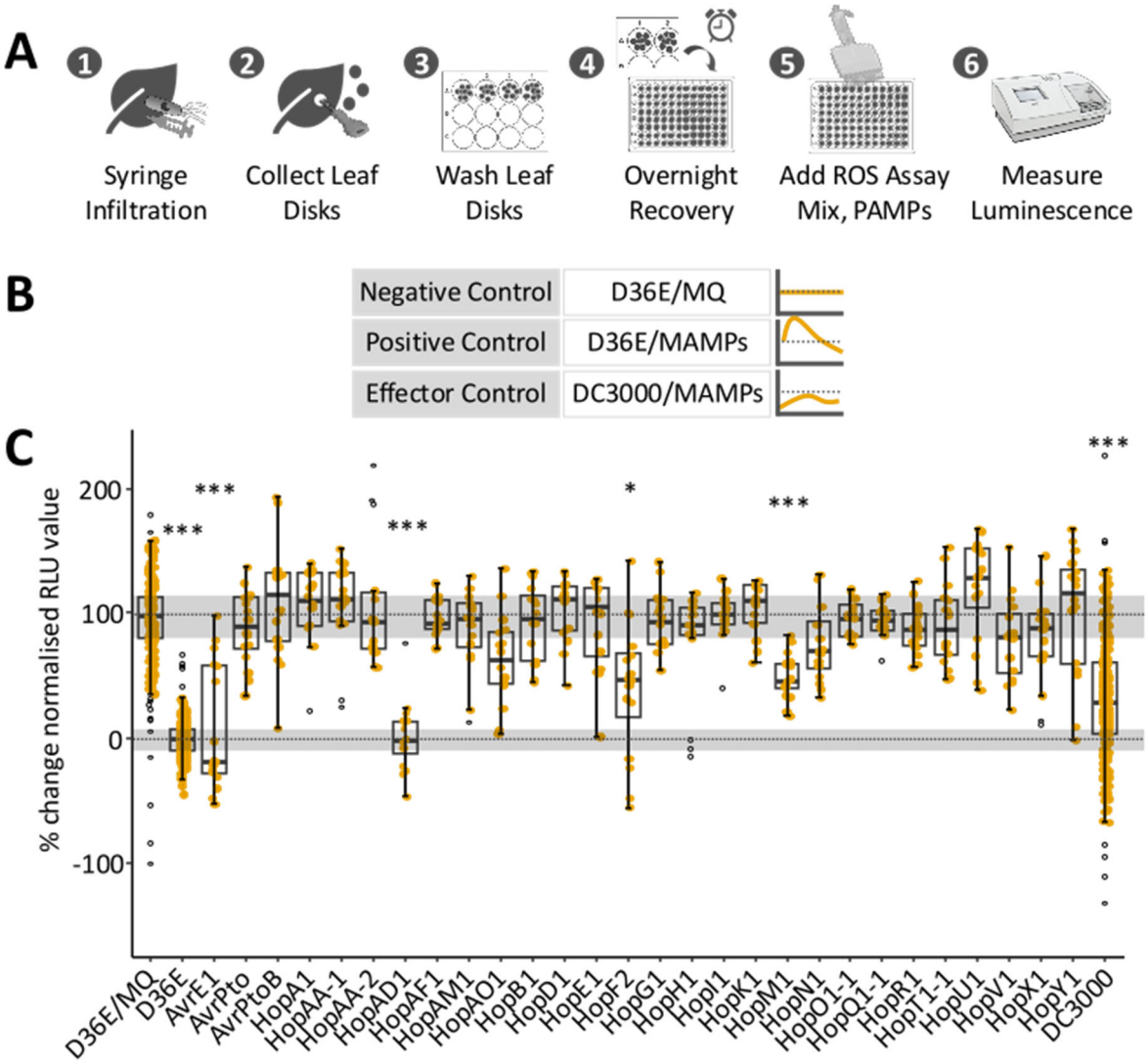

Figure 4: *AvrE1*, *HopAD1*, and *HopM1* can suppress the ROS burst in spinach when delivered by D36E. A) Overview of the experimental procedure used to analyse reactive oxygen species (ROS) bursts in spinach. Leaves were pre-infiltrated with D36E strains carrying individual effectors, followed by ROS burst elicitation using a MAMP mix. Chemiluminescence in relative light units (RLUs) was recorded as a measure of ROS production. **B)** Description of controls used in ROS burst assays: a negative control (D36E/MQ) in which leaves are pre-infiltrated with effectorless D36E and mock-elicited, a positive control (D36E/MAMPs) in which a ROS burst is triggered with a MAMP-mix derived from heat-lysed D36E bacterial cells in leaves pre-infiltrated with effectorless D36E, and a suppressed control (DC3000/MAMPs) in which a ROS burst is suppressed in leaves pre-infiltrated with DC3000. **C)** Quantification of ROS burst suppression following infiltration of D36E expressing 28 individual DC3000 effectors. The percent change in ROS burst was calculated relative to the negative control. One-way ANOVA followed by Dunnett's post-hoc test was applied to compare normalized and scaled RLU of D36E effector strains to the negative control. Asterisks indicate significant differences ($p < 0.001$, $p < 0.01$, $p < 0.05$; $n = 16$ leaf discs per treatment).

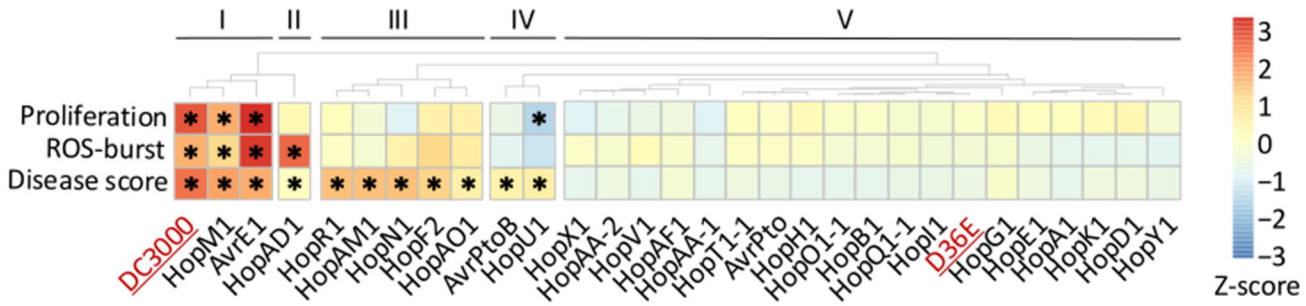

Figure 5: Systematic analysis of the functional effector screens highlights that D36E expressing *AvrE1* and *HopM1* restore DC3000-like phenotypes on spinach. Assay read-outs were Z-scaled to enable direct comparison of phenotypic outcomes across 28 individual DC3000 effectors expressed in D36E. Hierarchical clustering of Z-scaled values identified five distinct clusters (Cluster I – Cluster V), reflecting different phenotypic patterns. The largest group of 18 DC3000 effectors (Cluster V), did not significantly affect spinach in any of the assays, while *AvrE1* and *HopM1* appear as the most important contributors to DC3000-like symptoms (Cluster I). Asterisks (*) indicate significant effects ($p < 0.05$).

394 ## Material and Methods

395 ### Plant material

396 All *in planta* assays were conducted using the spinach cultivar Viroflay (Pop Vriend Seeds, The
397 Netherlands). Seeds were sown and plants were cultivated on Primasta® potting soil within a plant
398 growth room providing a stable environment (21˚C, 16 hr photoperiod, 70% relative humidity,
399 200 µmol m^{2} s^{-1} light intensity). Assays were initiated when the first true leaves were fully expanded,
400 and the second set of true leaves started development, typically occurring between 2.5 and 3 weeks post
401 sowing. To ensure consistency, phenotypically-similar plants were selected for all experiments.

402 ### *Pseudomonas* infiltration

403 To identify a suitable bacterium for T3SS-dependent effector delivery into spinach, we tested different
404 *Pseudomonas* strains. Preparation of bacterial cultures and infiltration was performed as previously
405 described with the following adaptations (Wei et al., 2013; Liu et al., 2015). Bacteria were grown for two
406 days on solid King's B medium (KB) supplemented with antibiotics at 28˚C (King et al., 1954). Antibiotic
407 resistances and their concentrations are listed in Table S2. Bacteria were re-streaked to new KB agar
408 plates 2 days prior to infiltration (28˚C). For infiltration, bacteria were scraped off the KB agar plates and
409 suspended in infiltration medium (10 mM $MgSO_4$, 50 µl/l Coatosil 1220 surfactant in MilliQ (MQ) water).
410 Bacteria were infiltrated from the abaxial side of fully expanded spinach leaves with a needleless syringe.
411 Infiltrated spinach plants were placed in trays and covered from the light before transfer to the climate
412 chamber. The cover was removed after one day, exposing the plants to the light conditions. Screening
413 for symptom development and bacterial proliferation were performed as described below.

414 ## Generating the D36E single effector library

415 For single effector screens in this study, we obtained the DC3000 single effector library in pENTR/SD/D-
416 TOPO backbones and the matching Gateway destination vector pCPP5372 via the non-profit plasmid
417 repository Addgene (Wei et al., 2018). Single *Escherichia coli* colonies were picked and grown in
418 overnight liquid Luria-Bertani (LB) medium supplemented with selective antibiotics (Table S1, S2, S3).
419 Plasmids were isolated using the QIAprep® Spin Miniprep Kit (Qiagen), followed by Sanger sequencing
420 with the M13 forward primers to confirm effector identity (Table S4). We mobilised DC3000 effector
421 genes into *pCPP5372* by Gateway® LR cloning as previously described (Wei et al., 2018). For propagation,
422 plasmids were transformed into Top10 *E. coli* cells and grown on LB agar plates with selective antibiotics
423 (Table S1, S2, S3). We selected positive colonies by colony-check PCR using effector-specific reverse
424 primers and the pCPP5372_pre_attR1 forward primer (Table S4). Effector expression plasmids were
425 mobilised from *E. coli* into D36E by triparental mating using the pRK2013 *E. coli* HB101 with the *pRK2013*
426 helper plasmid (Table S1).

427 ## Visual symptom scoring

428 To assess the visual development of symptoms, *Pseudomonas* strains were prepared and infiltrated as
429 described above. After infiltration, plants were grown until visual assessment of symptoms at 6-7 dpi. To
430 evaluate the symptoms of the single effector library on spinach, we infiltrated each leaf with the negative
431 control D36E and the positive control DC3000, alongside D36E carrying individual effectors. D36E does
432 not trigger symptoms while DC3000 does. The two remaining infiltrated sites per leaf were infiltrated
433 with the individual effector lines. We established a symptom scoring matrix ranging from symptom score
434 0 to symptom score 4, corresponding to no symptoms (0), mild chlorosis (1), clear chlorosis (2), signs of
435 necrosis (3) and clear necrosis (4) (Figure 2, S3). A Fisher's Exact test was applied to compare incidences

436 of symptom-positive infiltration sites (symptom score >1) against the incidence of symptom-free
437 infiltrated sites (symptom score <2). The number of infiltration sites showing a specific score was plotted
438 using the *R* package *ggplot2* (Wickham, 2016; Team;, 2021).

439 D36E proliferation assays

440 To better understand the connection between visual symptom and bacterial titres of *Pseudomonas*
441 strains, we assessed bacterial proliferation as a proxy for virulence by evaluating bacterial titres. We
442 adapted the published protocol by Liu et al. (2015) (Liu et al., 2015). First, spinach leaves were infiltrated
443 with *Pseudomonas* strains as described above. Then, infiltrated leaves were allowed to dry for 1.5 to 2
444 hours before collecting 0 dpi samples. These samples were used to verify successful, homogenous
445 infiltration. Three leaf discs (4 mm diameter) per infiltration sites were collected in 500 µl infiltration
446 medium containing three glass beads (2 mm). Bacterial cells were extracted from spinach tissue by
447 applying tissue lysis using the TissueLyser II (Qiagen, 85300) until leaf discs were completely
448 homogenized (twice 2 min, 30 hz s^{-1}). We prepared 10-fold serial dilutions of homogenized samples in
449 infiltration medium using 96-well plates. From all dilution steps, 5-µl droplets were transferred to square
450 KB agar plates with appropriate antibiotics (Table S1, S2). Droplets were allowed to dry, and plates were
451 then sealed with Parafilm (Bemis, PM996) and incubated for 1.5 to 2 days at 28°C until colonies were
452 clearly visible. Bacterial titres were estimated by counting colony forming units (CFUs) on KB agar plates.
453 CFUs counts at the highest dilution level with >3 three colonies, were used to calculate the number of
454 CFUs per cm^2 spinach leaf.

455 Data were processed in *R* and plotted in *ggplot2* (Wickham, 2016). For statistical analysis of initial
456 *Pseudomonas* screens (Figure 1), we assessed differences in proliferation between 0 dpi and 2 dpi using
457 a two-tailed t-test. For statistical analysis of the single effector library screens at 2 dpi, relative to the

458 D36E negative control, we applied an ANOVA followed by a Tukey post-hoc test. Scripts and raw data
459 are available on GitHub.

460 D36E-compatible ROS burst assays in spinach

461 We modified the ROS burst assay from (Johanndrees et al., 2022), based on (Bisceglia et al., 2015) to
462 make it compatible with the D36E effector delivery system in spinach. First, we identified elicitors for
463 ROS bursts in spinach. Spinach leaf discs (4 mm diameter) were harvested from 2.5-3-week-old plants
464 and washed trice in MQ water (30 min, gentle shaking). Discs were arranged on a 96-well plate (Greiner
465 Bio-One; 655075) in 200 µl MQ water, wrapped in aluminium foil to shield from light, and incubated at
466 21°C overnight. MQ was replaced with the luminol analogue L-012 sodium salt (Merck SML2236, final
467 concentration 180 µM) and horseradish peroxidase (Merck; P8125-5KU, 0.125 units per reaction)
468 solution. To each sample well, 50 µL elicitor solution was added at concentrations specified in Table S5.
469 We tested chitin, flg22, nlp24 and heat-lysed *P. effusa* race-1 sporangia (15 min, 100°C; *Pe1* sporangia)
470 and heat-lysed D36E cells (15 min, 100°C; MAMP-mix). Additional details on elicitors can be found in
471 Table S5. Chemiluminescence was measured every 2.5 min in a GloMax® 96 Microplate Luminometer
472 (Promega).

473 To investigate the impact of effectors on the ROS burst in spinach using the D36E effector delivery
474 system, we first established the proper controls. Bacteria were cultivated and infiltrated at 0 dpi as
475 described above. Infiltrated spinach plants were dried for 1.5 to 2 hours before proceeding with the ROS
476 assay protocol as described above. D36E/MQ was established as negative control, D36E/MAMPs as
477 positive control, DC3000/MAMPs as effector-positive control which suppresses ROS bursts (Figure S5,
478 S6, S7). To compare ROS burst assays, $\log_2$ of raw Relative Light Units (RLUs) were calculated and plotted
479 using *ggplot2* in R (Wickham, 2016). Additional features, time to peak ROS scores, peak ROS score and

480 total ROS scores, were calculated using Python 3.10 (van Rossum and Drake, 2009). To screen the
481 complete single effector library for alterations in MAMP-mix elicited ROS bursts, all three controls were
482 included. To analyse the variable results of single effector library screens, we processed, normalised and
483 transformed raw RLUs in Python 3.10 with *pandas* version 1.5 using the internal positive and negative
484 controls for scaling (van Rossum and Drake, 2009; team, 2020). Statistical analysis using ANOVA followed
485 by a Dunnett's post hoc test and visualization was conducted in *R* using *ggplot2* (Wickham, 2016; Team;,
486 2021). All scripts and raw data available on GitHub.

487 Systematic analysis of single effector library screens on spinach

488 We constructed a heatmap using the *pheatmap* package in *R* (Kolde, 2018; Team;, 2021). Phenotypic
489 outcomes are presented by extraction of representative single-values from visual symptom scoring,
490 bacterial proliferation assays and ROS burst assays. ROS burst values were inverted by multiplication
491 with -1 to allow for intuitive presentation of effector contribution to symptoms. We clustered rows using
492 the Euclidean distance metric combined with complete linkage mapping for hierarchical clustering
493 (*pheatmap* default). To facilitate an ordered discussion of the heatmap, we manually rotated the leaves
494 of the dendrogram. Linear regression was conducted by calculating R^2 values using a linear model,
495 corresponding p-values are presented. Results were plotted in *R* using *ggplot2* (Wickham, 2016; Team;,
496 2021). Scripts and raw data are available on GitHub.

Acknowledgments

This project was financially supported by the TopSector TKI Tuinbouw & Uitgangsmaterialen, the Netherlands, and four private spinach breeding companies: Enza Zaden Research & Development B.V. (NL), Pop Vriend Seeds (subsidiary of KWS Vegetables BV) (NL), Rijk Zwaan Breeding B.V. (NL), and Syngenta (NL).

We are grateful for the generosity of the research community in sharing bacterial strains. Special thanks to Alan Collmer, Professor Emeritus of Cornell University, and Wei Zhang, Cornell University, for providing the DC3000 D36E and D28E strains, and to Jeff Chang of Oregon State University for sharing the EtHAn strain.

507 ## References

508 Alfano, J.R., Charkowski, A.O., Deng, W.-L., Badel, J.L., Petnicki-Ocwieja, T., van Dijk, K., and Collmer, A. 2000. The *Pseudomonas*
509 *syringae* Hrp pathogenicity island has a tripartite mosaic structure composed of a cluster of type III secretion genes
510 bounded by exchangeable effector and conserved effector loci that contribute to parasitic fitness and pathogenicity
511 in plants. Proceedings of the National Academy of Sciences 97:4856-4861.
512 Arnold, D.L., Lovell, H.C., Jackson, R.W., and Mansfield, J.W. 2011. Pseudomonas syringae pv. phaseolicola: from 'has bean' to
513 supermodel. Molecular Plant Pathology 12:617-627.
514 Badel, J.L., Shimizu, R., Oh, H.-S., and Collmer, A. 2006. A Pseudomonas syringae pv. tomato avrE1/hopM1 Mutant Is Severely
515 Reduced in Growth and Lesion Formation in Tomato. Molecular Plant-Microbe Interactions 19:99-111.
516 Baltrus, D.A., Nishimura, M.T., Romanchuk, A., Chang, J.H., Mukhtar, M.S., Cherkis, K., Roach, J., Grant, S.R., Jones, C.D., and
517 Dangl, J.L. 2011. Dynamic Evolution of Pathogenicity Revealed by Sequencing and Comparative Genomics of 19
518 Pseudomonas syringae Isolates. PLOS Pathogens 7:e1002132.
519 Bhattarai, G., Yang, W., Shi, A., Feng, C., Dhillon, B., Correll, J.C., and Mou, B. 2021. High resolution mapping and candidate
520 gene identification of downy mildew race 16 resistance in spinach. BMC Genomics 22:478.
521 Bisceglia, N.G., Gravino, M., and Savatin, D.V. 2015. Luminol-based assay for detection of immunity elicitor-induced hydrogen
522 peroxide production in Arabidopsis thaliana leaves. Bio-protocol 5:e1685-e1685.
523 Buell, C.R., Joardar, V., Lindeberg, M., Selengut, J., Paulsen, I.T., Gwinn, M.L., Dodson, R.J., Deboy, R.T., Durkin, A.S., Kolonay,
524 J.F., Madupu, R., Daugherty, S., Brinkac, L., Beanan, M.J., Haft, D.H., Nelson, W.C., Davidsen, T., Zafar, N., Zhou, L., Liu,
525 J., Yuan, Q., Khouri, H., Fedorova, N., Tran, B., Russell, D., Berry, K., Utterback, T., Van Aken, S.E., Feldblyum, T.V.,
526 D'Ascenzo, M., Deng, W.-L., Ramos, A.R., Alfano, J.R., Cartinhour, S., Chatterjee, A.K., Delaney, T.P., Lazarowitz, S.G.,
527 Martin, G.B., Schneider, D.J., Tang, X., Bender, C.L., White, O., Fraser, C.M., and Collmer, A. 2003. The complete
528 genome sequence of the *Arabidopsis* and tomato pathogen *Pseudomonas syringae* pv. *tomato* DC3000. Proceedings
529 of the National Academy of Sciences 100:10181-10186.
530 Cai, X., Sun, X., Xu, C., Sun, H., Wang, X., Ge, C., Zhang, Z., Wang, Q., Fei, Z., Jiao, C., and Wang, Q. 2021. Genomic analyses
531 provide insights into spinach domestication and the genetic basis of agronomic traits. Nature Communications
532 12:7246.
533 Chang, J.H., Urbach, J.M., Law, T.F., Arnold, L.W., Hu, A., Gombar, S., Grant, S.R., Ausubel, F.M., and Dangl, J.L. 2005. A high-
534 throughput, near-saturating screen for type III effector genes from Pseudomonas syringae. Proceedings of the
535 National Academy of Sciences 102:2549-2554.
536 Cheung AY. 2024. FERONIA: A Receptor Kinase at the Core of a Global Signaling Network. Annual Review of Plant Biology.
537 75(1):345-375.
538 Clark, K. J., Feng, C., Anchieta, A. G., Van Deynze, A., Correll, J. C., & Klosterman, S. J. 2024. Dual transcriptional characterization
539 of spinach and Peronospora effusa during resistant and susceptible race-cultivar interactions. BMC genomics, 25.1:
540 937.
541 Cunnac, S., Chakravarthy, S., Kvitko, B.H., Russell, A.B., Martin, G.B., and Collmer, A. 2011. Genetic disassembly and
542 combinatorial reassembly identify a minimal functional repertoire of type III effectors in Pseudomonas syringae.
543 Proceedings of the National Academy of Sciences 108:2975-2980.
544 DebRoy, S., Thilmony, R., Kwack, Y.-B., Nomura, K., and He, S.Y. 2004. A family of conserved bacterial effectors inhibits salicylic
545 acid-mediated basal immunity and promotes disease necrosis in plants. Proceedings of the National Academy of
546 Sciences 101:9927-9932.
547 Ditta, G., Stanfield, S., Corbin, D., and Helinski, D.R. 1980. Broad host range DNA cloning system for gram-negative bacteria:
548 construction of a gene bank of Rhizobium meliloti. Proceedings of the National Academy of Sciences 77:7347-7351.
549 Fabro, G., Steinbrenner, J., Coates, M., Ishaque, N., Baxter, L., Studholme, D.J., Körner, E., Allen, R.L., Piquerez, S.J.M., Rougon-
550 Cardoso, A., Greenshields, D., Lei, R., Badel, J.L., Caillaud, M.-C., Sohn, K.-H., Van den Ackerveken, G., Parker, J.E.,
551 Beynon, J., and Jones, J.D.G. 2011. Multiple Candidate Effectors from the Oomycete Pathogen Hyaloperonospora
552 arabidopsidis Suppress Host Plant Immunity. PLOS Pathogens 7:e1002348.
553 Fletcher, K., Shin, O.-H., Clark, K.J., Feng, C., Putman, A.I., Correll, J.C., Klosterman, S.J., Van Deynze, A., and Michelmore, R.W.
554 2022. Ancestral Chromosomes for Family Peronosporaceae Inferred from a Telomere-to-Telomere Genome Assembly
555 of Peronospora effusa. Molecular Plant-Microbe Interactions 35:450-463.
556 Gao, S., Lu, T., She, H., Xu, Z., Zhang, H., Liu, Z., and Qian, W. 2022. Fine Mapping and Identification of a Candidate Gene of
557 Downy Mildew Resistance, RPF2, in Spinach (Spinacia oleracea L.). International Journal of Molecular Sciences 23.

558 Hulse-Kemp, A.M., Bostan, H., Chen, S., Ashrafi, H., Stoffel, K., Sanseverino, W., Li, L., Cheng, S., Schatz, M.C., Garvin, T., du Toit,
559 L.J., Tseng, E., Chin, J., Iorizzo, M., and Van Deynze, A. 2021. An anchored chromosome-scale genome assembly of
560 spinach improves annotation and reveals extensive gene rearrangements in euasterids. The Plant Genome 14:e20101.
561 Jayaraman, J., Yoon, M., Applegate, E.R., Stroud, E.A., and Templeton, M.D. 2020. AvrE1 and HopR1 from Pseudomonas
562 syringae pv. actinidiae are additively required for full virulence on kiwifruit. Molecular plant pathology 21:1467-1480.
563 Johanndrees, O., Baggs, E.L., Uhlmann, C., Locci, F., Läßle, H.L., Melkonian, K., Käufer, K., Dongus, J.A., Nakagami, H., Krasileva,
564 K.V., Parker, J.E., and Lapin, D. 2022. Variation in plant Toll/Interleukin-1 receptor domain protein dependence on
565 ENHANCED DISEASE SUSCEPTIBILITY 1. Plant Physiology 191:626-642.
566 Jones, J.D.G., and Dangl, J.L. 2006. The plant immune system. Nature 444:323-329.
567 Jwa, N.S., and Hwang, B.K. 2017. Convergent Evolution of Pathogen Effectors toward Reactive Oxygen Species Signaling
568 Networks in Plants. Frontiers in Plant Science 8:1687.
569 Kandel, S.L., Hulse-Kemp, A.M., Stoffel, K., Koike, S.T., Shi, A., Mou, B., Van Deynze, A., and Klosterman, S.J. 2020. Transcriptional
570 analyses of differential cultivars during resistant and susceptible interactions with Peronospora effusa, the causal
571 agent of spinach downy mildew. Scientific reports 10:6719-6719.
572 Kandel, S.L., Mou, B., Shishkoff, N., Shi, A., Subbarao, K.V., and Klosterman, S.J. 2019. Spinach Downy Mildew: Advances in Our
573 Understanding of the Disease Cycle and Prospects for Disease Management. Plant Disease 103:791-803.
574 King, E. O., Ward, M. K., & Raney, D. E. 1954. Two simple media for the demonstration of pyocyanin and fluorescin. The Journal
575 of laboratory and clinical medicine, 44.2:301-307.
576 Klein, J., Neilen, M., van Verk, M., Dutilh, B.E., and Van den Ackerveken, G. 2020. Genome reconstruction of the non-culturable
577 spinach downy mildew Peronospora effusa by metagenome filtering. PLoS ONE 15:e0225808.
578 Kolde, R. (2018). Pretty Heatmaps.
579 Krasileva, K.V., Zheng, C., Leonelli, L., Goritschnig, S., Dahlbeck, D., and Staskawicz, B.J. 2011. Global analysis of
580 Arabidopsis/downy mildew interactions reveals prevalence of incomplete resistance and rapid evolution of pathogen
581 recognition. PLOS ONE 6:e28765.
582 Kvitko, B.H., Park, D.H., Velásquez, A.C., Wei, C.F., Russell, A.B., Martin, G.B., Schneider, D.J., and Collmer, A. 2009. Deletions in
583 the repertoire of Pseudomonas syringae pv. tomato DC3000 type III secretion effector genes reveal functional overlap
584 among effectors. PLoS Pathog 5:e1000388.
585 Liu, X., Sun, Y., Kørner, C.J., Du, X., Vollmer, M.E., and Pajerowska-Mukhtar, K.M. 2015. Bacterial Leaf Infiltration Assay for Fine
586 Characterization of Plant Defense Responses using the Arabidopsis thaliana-Pseudomonas syringae Pathosystem.
587 Journal of Visualized Experiments.
588 Liu, Y., Zeng, Z., Zhang, Y.-M., Li, Q., Jiang, X.-M., Jiang, Z., Tang, J.-H., Chen, D., Wang, Q., Chen, J.-Q., and Shao, Z.-Q. 2021. An
589 angiosperm NLR Atlas reveals that NLR gene reduction is associated with ecological specialization and signal
590 transduction component deletion. Molecular Plant 14:2015-2031.
591 Lozano-Durán, R., Bourdais, G., He, S.Y., and Robatzek, S. 2014. The bacterial effector HopM1 suppresses PAMP-triggered
592 oxidative burst and stomatal immunity. New Phytologist 202:259-269.
593 Lu, X., Kracher, B., Saur, I.M.L., Bauer, S., Ellwood, S.R., Wise, R., Yaeno, T., Maekawa, T., and Schulze-Lefert, P. 2016. Allelic
594 barley MLA immune receptors recognize sequence-unrelated avirulence effectors of the powdery mildew pathogen.
595 Proceedings of the National Academy of Sciences 113:E6486-E6495.
596 Mersmann, S., Bourdais, G., Rietz, S., and Robatzek, S. 2010. Ethylene signaling regulates accumulation of the FLS2 receptor
597 and is required for the oxidative burst contributing to plant immunity. Plant Physiology 154:391-400.
598 Neilen, M. (2020). RxLR and CRN effectors of the spinach downy mildew Peronospora effusa and their interacting plant
599 proteins. In Plant-Microbe Interactions (Utrecht: Utrecht University).
600 Ngou, B.P.M., Ahn, H.-K., Ding, P., and Jones, J.D.G. 2021. Mutual potentiation of plant immunity by cell-surface and
601 intracellular receptors. Nature 592:110-115.
602 Ngou, B.P.M., Ding, P., and Jones, J.D.G. 2022. Thirty years of resistance: Zig-zag through the plant immune system. The Plant
603 Cell 34:1447-1478.
604 Nomura, K., Andreazza, F., Cheng, J., Dong, K., Zhou, P., and He, S.Y. 2023. Bacterial pathogens deliver water- and solute-
605 permeable channels to plant cells. Nature.
606 Nomura, K., DebRoy, S., Lee, Y.H., Pumplin, N., Jones, J., and He, S.Y. 2006. A bacterial virulence protein suppresses host innate
607 immunity to cause plant disease. Science 313:220-223.
608 Oh, H.S., Kvitko, B.H., Morello, J.E., and Collmer, A. 2007. Pseudomonas syringae lytic transglycosylases coregulated with the
609 type III secretion system contribute to the translocation of effector proteins into plant cells. Journal of Bacteriology
610 189:8277-8289.

611 Oome, S., Raaymakers, T., Cabral, A., Samwel, S., Böhm, H., Albert, I., Nürnberger, T., and Van den Ackerveken, G. 2014. Nep1-
612 like proteins from three kingdoms of life act as a microbe-associated molecular pattern in Arabidopsis. Proceedings
613 of the National Academy of Sciences 111.
614 Pelgrom, A.J.E., Eikelhof, J., Elberse, J., Meisrimler, C.-N., Raedts, R., Klein, J., and Van den Ackerveken, G. 2019. Recognition of
615 lettuce downy mildew effector BLR38 in Lactuca serriola LS102 requires two unlinked loci. Molecular Plant Pathology
616 20:240-253.
617 R Core Team. 2021. R: A Language and Environment for Statistical Computing (Vienna, Austria: R Foundation for Statistical
618 Computing).
619 Ribera, A., Bai, Y., Wolters, A.-M.A., van Treuren, R., and Kik, C. 2020. A review on the genetic resources, domestication and
620 breeding history of spinach (Spinacia oleracea L.). Euphytica 216:48.
621 Roussin-Léveillée, C., Lajeunesse, G., St-Amand, M., Veerapen, V.P., Silva-Martins, G., Nomura, K., Brassard, S., Bolaji, A., He,
622 S.Y., and Moffett, P. 2022. Evolutionarily conserved bacterial effectors hijack abscisic acid signaling to induce an
623 aqueous environment in the apoplast. Cell Host Microbe 30:489-501.e484.
624 Rustgi, S., Naveed, S., Windham, J., Zhang, H., and Demirer, G.S. 2022. Plant biomacromolecule delivery methods in the 21st
625 century. Frontiers in Genome Editing 4.
626 Sánchez-Vallet, A., Mesters, J.R., and Thomma, B.P.H.J. 2015. The battle for chitin recognition in plant-microbe interactions.
627 FEMS Microbiology Reviews 39:171-183.
628 Skiadas, P., Klein, J., Quiroz-Monnens, T., Elberse, J., de Jonge, R., Van den Ackerveken, G., and Seidl, M.F. 2022. Sexual
629 reproduction contributes to the evolution of resistance-breaking isolates of the spinach pathogen Peronospora effusa.
630 Environmental Microbiology 24:1622-1637.
631 Skiadas, P., Riera Vidal, S., Dommisse, J., Mendel, M.N., Elberse, J., Van den Ackerveken, G., de Jonge, R. and Seidl, M.F., 2024.
632 Pangenome graph analysis reveals extensive effector copy-number variation in spinach downy mildew. PLoS
633 Genetics, 20.10:1011452.
634 The pandas development team. 2020. pandas-dev/pandas: Pandas; (Zenodo).
635 Thomas, W.J., Thireault, C.A., Kimbrel, J.A., and Chang, J.H. 2009. Recombineering and stable integration of the Pseudomonas
636 syringae pv. syringae 61 hrp/hrc cluster into the genome of the soil bacterium Pseudomonas fluorescens Pf0-1. The
637 Plant Journal 60:919-928.
638 Upadhyaya, N., Mago, R., Staskawicz, B., Ayliffe, M., Ellis, J., and Dodds, P. 2013. A Bacterial Type III Secretion Assay for Delivery
639 of Fungal Effector Proteins into Wheat. Molecular Plant-Microbe Interactions 27.
640 Üstün, S., Sheikh, A., Gimenez-Ibanez, S., Jones, A., Ntoukakis, V., and Börnke, F. 2016. The Proteasome Acts as a Hub for Plant
641 Immunity and Is Targeted by Pseudomonas Type III Effectors Plant Physiology 172:1941-1958.
642 van Rossum, G., and Drake, F.L. (2009). Python 3 Reference Manual (Scotts Valley, CA: CreateSpace).
643 Wang, Y., Pruitt, R.N., Nürnberger, T., and Wang, Y. 2022. Evasion of plant immunity by microbial pathogens. Nature Reviews
644 Microbiology 20:449-464.
645 Wei, H.L., and Collmer, A. 2018. Defining essential processes in plant pathogenesis with Pseudomonas syringae pv. tomato
646 DC3000 disarmed polymutants and a subset of key type III effectors. Molecular Plant Pathology 19:1779-1794.
647 Wei, H.L., Chakravarthy, S., Mathieu, J., Helmann, T.C., Stodghill, P., Swingle, B., Martin, G.B., and Collmer, A. 2015.
648 Pseudomonas syringae pv. tomato DC3000 Type III Secretion Effector Polymutants Reveal an Interplay between
649 HopAD1 and AvrPtoB. Cell Host Microbe 17:752-762.
650 Wei, H.-L., Chakravarthy, S., Worley, J.N., and Collmer, A. 2013. Consequences of flagellin export through the type III secretion
651 system of Pseudomonas syringae reveal a major difference in the innate immune systems of mammals and the model
652 plant Nicotiana benthamiana. Cellular Microbiology 15:601-618.
653 Wei, H.L., Zhang, W., and Collmer, A. 2018. Modular Study of the Type III Effector Repertoire in Pseudomonas syringae pv.
654 tomato DC3000 Reveals a Matrix of Effector Interplay in Pathogenesis. Cell reports 23:1630-1638.
655 Wickham, H. 2016. ggplot2: Elegant Graphics for Data Analysis. Springer-Verlag New York.
656 Xin, X.-F., Nomura, K., Aung, K., Velásquez, A.C., Yao, J., Boutrot, F., Chang, J.H., Zipfel, C., and He, S.Y. 2016. Bacteria establish
657 an aqueous living space in plants crucial for virulence. Nature 539:524-529.
658 Xu, C., Jiao, C., Sun, H., Cai, X., Wang, X., Ge, C., Zheng, Y., Liu, W., Sun, X., Xu, Y., Deng, J., Zhang, Z., Huang, S., Dai, S., Mou, B.,
659 Wang, Q., Fei, Z., and Wang, Q. 2017. Draft genome of spinach and transcriptome diversity of 120 Spinacia accessions.
660 Nature Communications 8:15275.
661 Yuan, J., and He, S.Y. 1996. The Pseudomonas syringae Hrp regulation and secretion system controls the production and
662 secretion of multiple extracellular proteins. Journal of Bacteriology 178:6399-6402.

663 Yuan, M., Jiang, Z., Bi, G., Nomura, K., Liu, M., Wang, Y., Cai, B., Zhou, J.-M., He, S.Y., and Xin, X.-F. 2021. Pattern-recognition
664 receptors are required for NLR-mediated plant immunity. Nature 592:105-109.
665 Zhang, L., Hua, C., Janocha, D., Fliegmann, J., and Nürnberger, T. 2023a. Plant cell surface immune receptors—Novel insights
666 into function and evolution. Current Opinion in Plant Biology 74:102384.
667 Zhang, Y., Qiu, L., Zhang, Y., Wang, Y., Fu, C., Dai, S. and Sun, M., 2024. A high-efficiency transient expression system mediated
668 by Agrobacterium tumefaciens in Spinacia oleracea leaves. Plant Methods, 20.1:100.
669

670 Supplementary Material

671

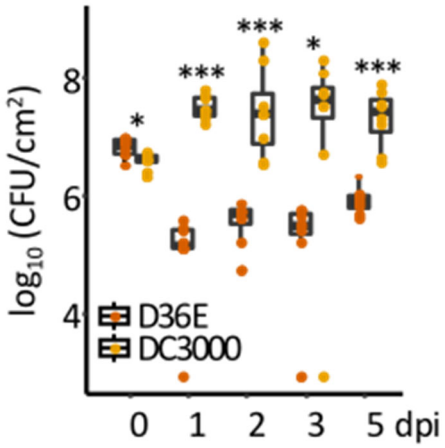

672

673 **Figure S1: DC3000 and D36E titres stabilize at different levels between 1- and 5-day post-infiltration**
674 **(dpi) in spinach.** To evaluate whether bacterial populations stabilise, we infiltrated bacterial cultures at
675 0 days post-infiltration (dpi) at OD_{600} equal to 0.4 and tracked titres (colony-forming units or CFU) over
676 five days, sampling 0- 3 dpi and 5 dpi. The low variance at 0 dpi is indicative of proper technical
677 reproducibility. Already at 1 dpi it becomes clear that DC3000 cells actively proliferate in spinach while
678 the titres of D36E decrease. Afterwards, both populations appear to stabilize and the difference between
679 titres remains significant until the end of the experiment. For statistical analysis, we applied a two-tailed
680 t-test (*** $p < 0.001$, ** $p < 0.01$, * $p < 0.05$).

681

682

683

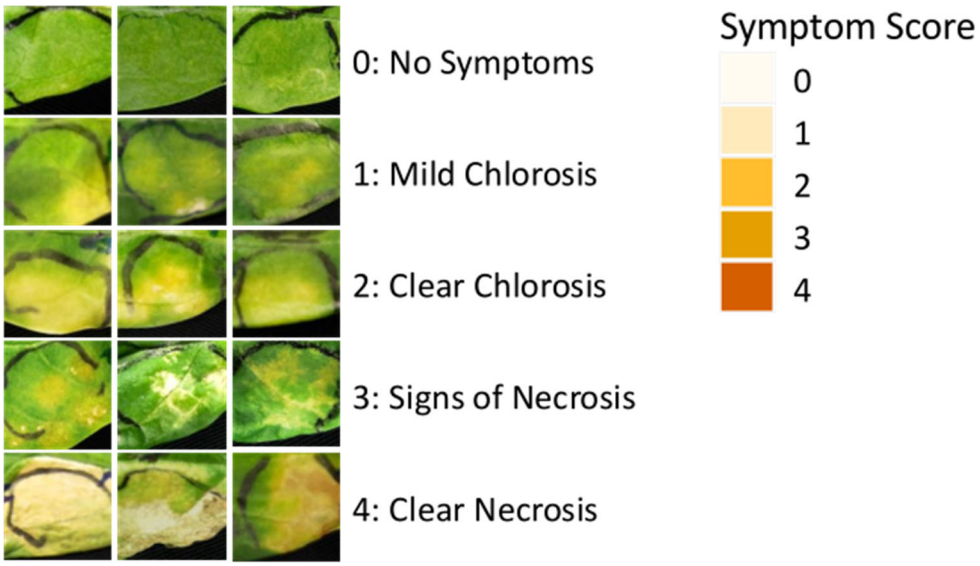

684

685 **Figure S2: Variation in visual symptoms and symptom scores.** We observed substantial variation in
686 symptoms on spinach following infiltration with *Pseudomonas* strains. To categorise visual symptoms
687 and capture the variation of symptoms, we devised a scoring matrix (Figure 2).

688

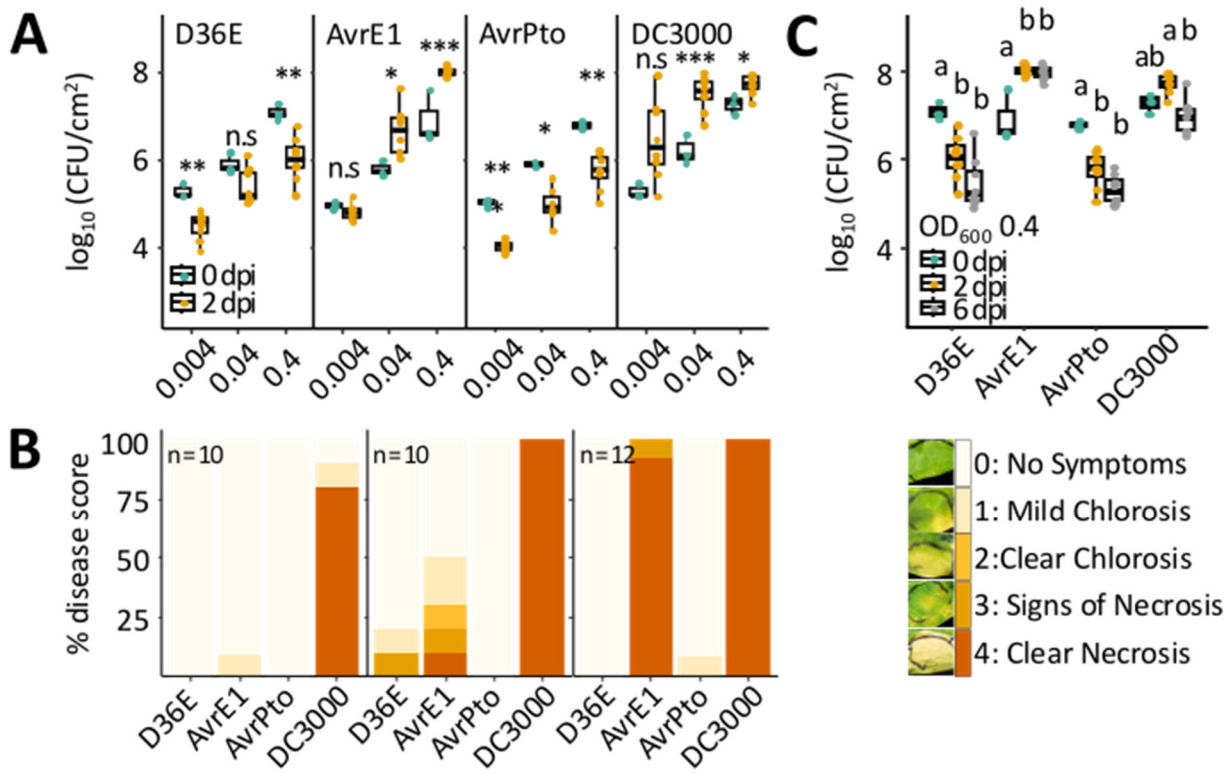

Figure S3: *Pseudomonas* titres and symptom development in spinach at varying inoculum densities and late timepoints. A) Bacterial titres develop similarly between 0-day post-infiltration (dpi) and 2 dpi across different inoculum densities. At OD_{600} equal to 0.004, *AvrE1* titres no longer increase between 0 dpi and 2 dpi. In contrast, DC3000 titres increase less than 1 order of magnitude at OD_{600} of 0.4 but increase around 2 orders of magnitude at OD_{600} of 0.04. **B)** Development of symptoms after infiltration of *Pseudomonas* strains at different inoculum densities at 6 dpi (left: OD_{600} equal to 0.004, middle: OD_{600} equal to 0.04, right: OD_{600} equal to 0.4). We scored symptoms in each infiltration site based on the presented symptom scoring matrix ranging from 0 (no symptoms) to 4 (necrotic symptoms). DC3000 causes severe, level 4 symptoms in most infiltration sites at all tested inoculum densities, while *AvrE1* triggered symptoms drop considerably at the two lowest inoculum densities. D36E and *AvrPto* do not cause visible symptoms. **C)** *Pseudomonas* titres at 0 dpi, 2 dpi and 6 dpi following infiltration at OD_{600} equal to 0.4. Titres of D36E and *AvrPto* decrease significantly over time, whereas *AvrE1* and DC3000 titres increase initially, but drop between 2 dpi and 6 dpi in the case of DC3000. We conducted a one-way ANOVA followed by Tukey's Honestly Significant Difference (HSD) test separately for each strain. Statistical differences are indicated by letters above the boxplots, with n = 3 infiltration sites per treatment.

707

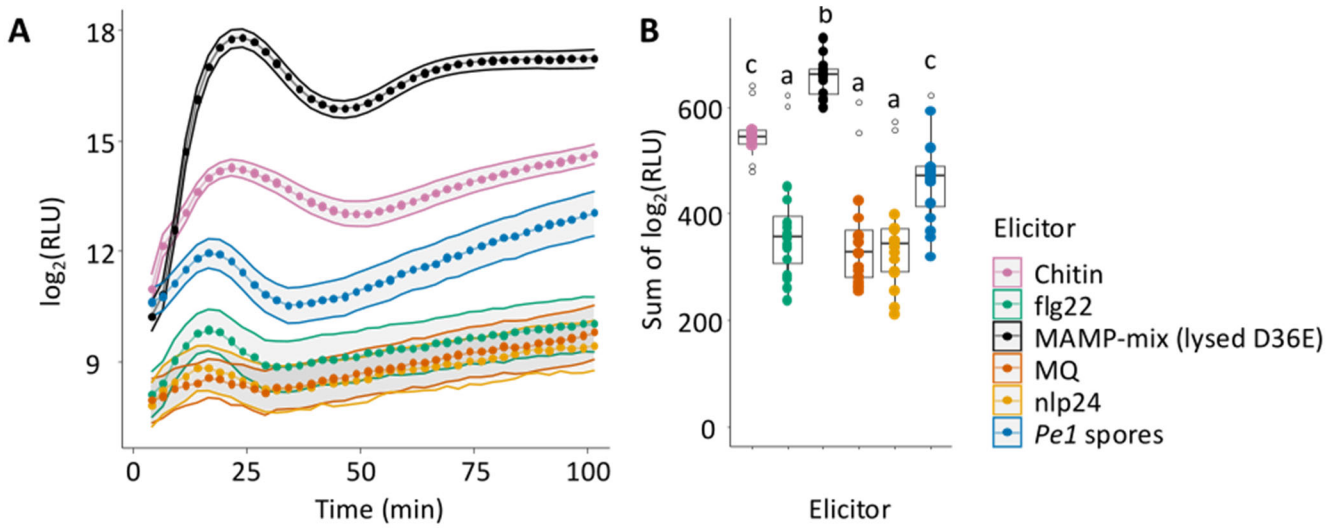

708

709 **Figure S4: Screening putative reactive oxygen species (ROS) burst elicitors on spinach.** We tested five
710 different elicitors for their ability to trigger a rapid ROS burst in spinach, measured as relative light units
711 (RLU). We chose the well-described MAMP-type elicitors chitin, flg22 and nlp24, and we included two
712 elicitor mixes, i.e.: heat-lysed D36E (MAMP-mix/MAMP) cells and heat-lysed *P. effusa race 1* (*Pe1*)
713 sporangia. We show results as a $\log_2$ transformed raw relative light units (RLUs) values (**A**), and the sum
714 of $\log_2$ transformed raw RLU values over the duration of the experiment (**B**). The MAMP-mix elicited the
715 strongest ROS burst (black), followed by chitin (pink), scoring in sum around 100 $\log_2$(RLU) lower.

716

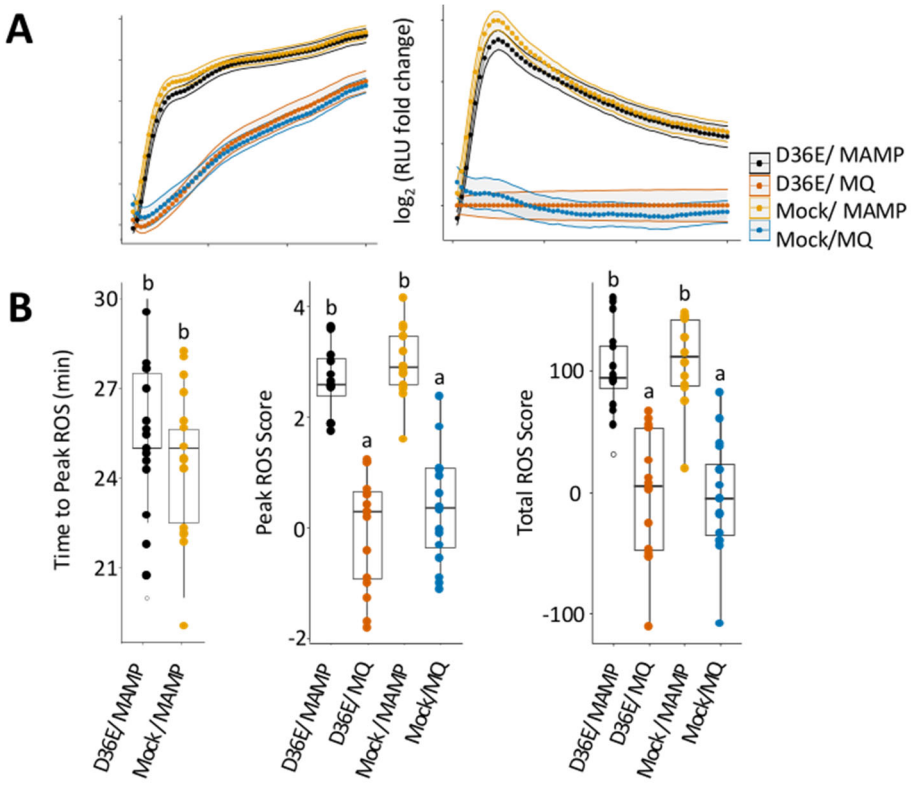

Figure S5: Establishing negative and positive controls for reactive oxygen species (ROS) burst assays on spinach in combination with the effectorless *Pseudomonas syringae pv. tomato* strain (D36E) delivery. A) To establish ROS burst negative and positive controls, we measured and compared ROS in relative light units (RLU) mock-infiltrated and non-elicited (mock/MQ) and mock-infiltrated and elicited (mock/MAMP) samples with D36E-infiltrated and non-elicited (D36E/MQ) and D36E-infiltrated and elicited (D36E/MAMP) samples. In both comparisons, D36E had no significant impact on ROS burst results, establishing D36E/MQ as a negative control and D36E/MAMPs as a positive control. For all treatments, we noted a consistent rise in ROS production over time, even in the absence of elicitation (**left**). We normalized our data for this steady increase in background ROS levels by calculating the fold change between the negative control D36E/MQ and measurements of other samples at each timepoint (measurement/control measurement) (**right**). Furthermore, the analysis revealed that no major changes in ROS production are to be expected after ~50 min, which we consequentially used as maximum time during effector screening. **B**) Boxplots display three parameters extracted from the time-resolved graphs depicted in **(A)** after transformation and normalization, i.e.: time to peak ROS (time to maximum ROS production) (**left**), peak ROS scores (maximum of measure ROS scores) (**middle**), and total ROS scores (sum of ROS scores over time) (**right**). Time to peak ROS does not show a statistically significant difference between mock-elicited and MAMP-mix-elicited samples. Peak ROS scores and total ROS scores show significant differences between mock-elicited and elicited samples but no difference between mock-infiltrated and D36E infiltrated samples, confirming the choice of controls for further use. We conducted statistical analysis using ANOVA, followed by Tukey's Honestly Significant Difference test ($p < 0.05$). Distinct letters denote significantly different groups.

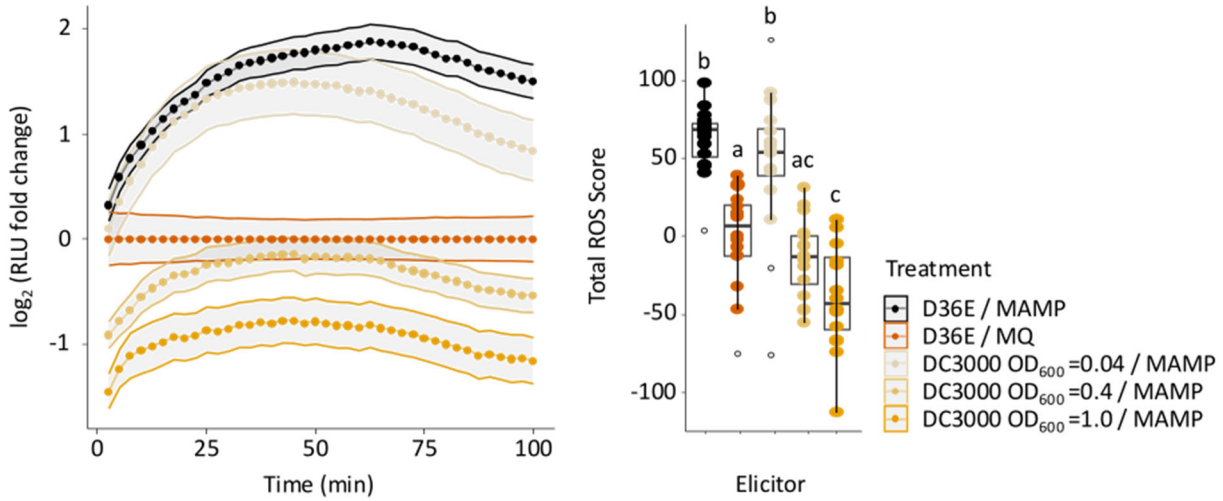

Figure S6: DC3000 supresses reactive oxygen species (ROS) bursts in spinach in a concentration-dependent manner. We infiltrated spinach with the ROS burst negative control D36E/MQ, the ROS burst positive control D36E/MAMP or DC3000 at different bacterial densities ranging from OD_{600} equal to 0.04, 0.4, to 1.0 plus the MAMP-mix. We show time-resolved graphs measuring ROS in relative light units (RLU) (**left**) and total ROS scores (**right**). Compared to the ROS burst negative control, D36E/MQ, DC3000 OD_{600} equal to 0.04 plus MAMP-mix showed only a trend, but no significant reduction of total ROS scores compared to D36E/MAMP, while DC3000 OD_{600} equal to 0.4 or equal to 1.0 plus MAMP-mix showed total ROS scores significantly lower than D36E/MAMP. Statistical analysis was conducted by ANOVA, followed by a Tukey's Honestly Significant Difference test ($p < 0.05$). Letters above the boxplots indicate statistically significant different groups

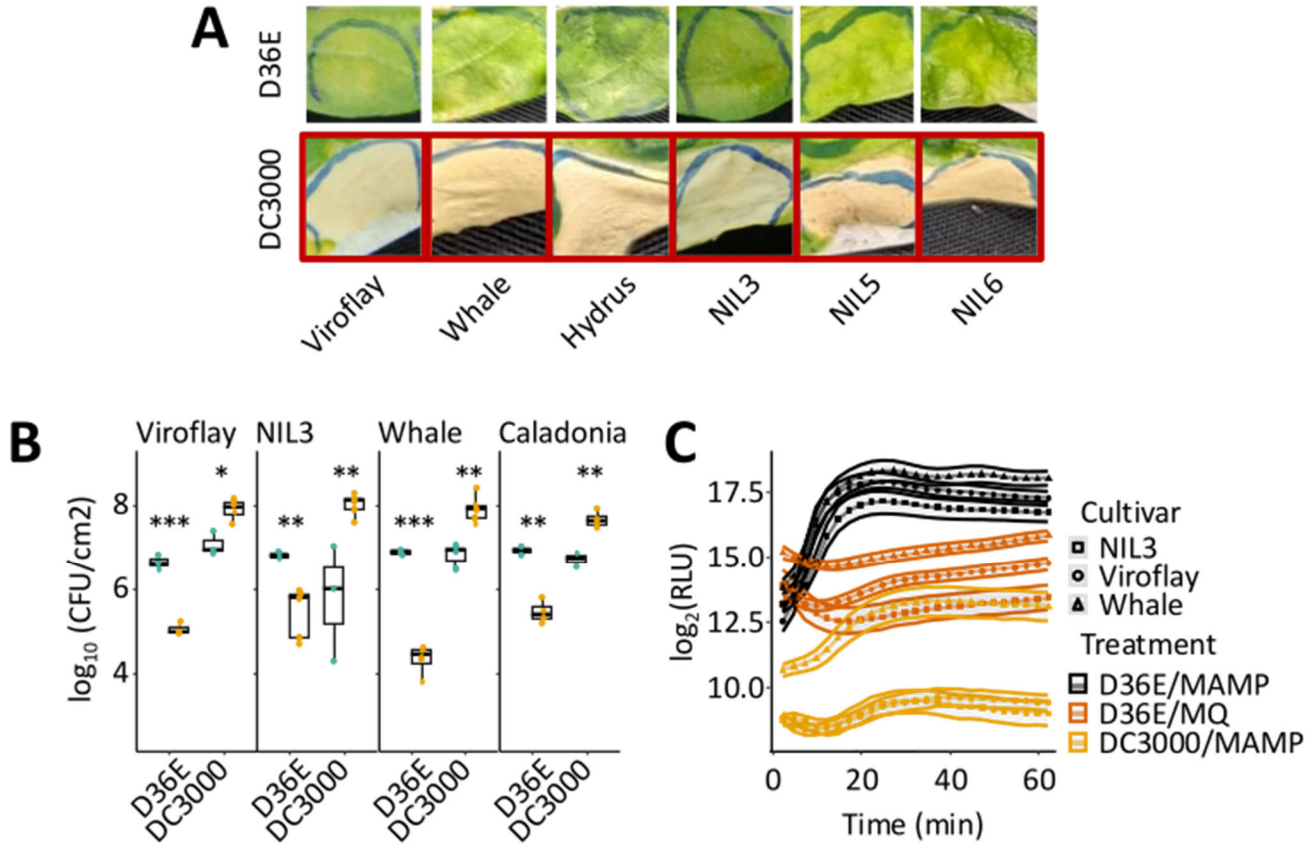

Figure S7: Different spinach cultivars react similarly to control treatments. We assessed if spinach cultivars differed in their response to control treatments with D36E or DC3000 in symptom development**,** bacterial proliferation or reactive oxygen species (ROS) bursts following MAMP elicitation. In **A)** we assessed symptom development in response to bacteria infiltration. All cultivars show a strong, cell-death/necrosis upon infiltration of DC3000 but not D36E. **B)** In the tested cultivars, D36E titres (colony-forming units or CFU) significantly decrease between 0-day post-infiltration (dpi) and 2 dpi, while DC3000 titres significantly increase over the same period. We applied a two-tailed t-test (*** $p < 0.001$, ** $p < 0.01$, * $p < 0.05$). **C)** One day prior to ROS elicitation with the MAMP mix, spinach was infiltrated with either D36E or DC3000 and ROS was measured in relative light units (RLU). In all three tested cultivars, D36E/MQ treatment resulted in stable or slightly increasing ROS levels over time. D36E/MAMPs treatment elicited a ROS burst followed by elevated ROS levels. In contrast, DC3000/MAMPs treatment reduced ROS levels relative to D36E/MQ, though absolute ROS levels varied among cultivars.

765

766

Table S1 Detailed information on the bacterial strains used in this study.

767

Strain	Description	Resistances	Reference
The Effector-to-Host Analyser (EtHAn)	*Pseudomonas fluorescens* Pf0-1 with the T3SS	Cm^r/Tet^r	(Thomas et al., 2009)
***Pseudomonas syringae pv. tomato* strain DC3000 (DC3000)**	Wildtype, natural pathogen of tomato	Rif^r	(Buell et al., 2003)
D28E	DC3000D28E = CUCPB5585	Rif^r /Sp^r/Ap^r/Sm^r	(Cunnac et al., 2011)
D36E	DC3000D36E = D35EΔ*hopAD1* = CUCPB6119	Rif^r / Sp^r	(Wei et al., 2015)
ΔCEL	DC3000Δ*CEL*	Rif^r / Sp^r	(Alfano et al., 2000)
hrcC	DC3000 *hrcC*$^{--}$ **=** T3SS$^-$	Rif^r	(Yuan and He, 1996)
***Pseudomonas syringae* pv. *Phaseolicola* (*Pph*)**	Wildtype, natural pathogen of bean	Kan^r	Kind gift of Dr. John W. Mansfield (Arnold et al., 2011)
***E.coli* DH5α**	n/a	n/a	n/a
***E.coli* ccdB survival**	*E. coli* strain used to propagate pCPP5372	n/a	n/a
***E.coli* Top10**	Invitrogen™ One Shot™ TOP10 Chemically Competent *E. coli*	n/a	ThermoFisher Scientific, C404010
E.coli* HB101 *pRK2013		Kan^r	(Ditta et al., 198

769

770

771

772

773

774

Table S2: Antibiotics used in this study including abbreviations and standard working concentrations

Antibiotic	Abbreviation	Working concentration (µg/ml)
Ampicillin	Ap	100
Carbenicillin	Cb	100
Chloramphenicol	Cm	10
Gentamycin	Gm	25
Kanamycin	Kan	50
Rifampicin	Rif	50
Spectinomycin	Sp	50
Streptomycin	Stp	50
Tetracycline	Tet	20

Table S3: Plasmids utilized in this study. Including references and plasmid-encoded antibiotic resistances.

Plasmid Name	Resistance	References
pCPP5372	GmR, CmR	(Oh et al., 2007)
DC300 Effector	**pENTR constructs (Wei, 2018)**	**Resistance**
AvrE1	pCPP5912*	Kan^r
AvrPto	pCPP5154	Kan^r
HopA1	pCPP5530	Kan^r
HopB1	pCPP5617	Kan^r
HopD1	pCPP5588	Kan^r
HopE1	pCPP5618	Kan^r
HopF2	pCPP5058*	Kan^r
HopG1	pCPP5238	Kan^r
HopH1	pCPP5306	Kan^r
HopI1	pCPP5571	Kan^r
HopK1	pCPP5099	Kan^r
HopM1	pCPP5233*	Kan^r
HopN1	pCPP5060*	Kan^r
HopO1-1	pCPP5910*	Kan^r
HopQ1-1	pCPP3373	Kan^r
HopR1	pCPP5951	Kan^r
HopT1-1	pCPP3416	Kan^r
HopU1	pCPP5328	Kan^r
HopV1	pCPP5741*	Kan^r
HopX1	pCPP5534	Kan^r
HopY1	pCPP3417	Kan^r
HopAA1-1	pCPP5107	Kan^r
HopAA1-2	pCPP5108	Kan^r
AvrPtoB	pCPP5616	Kan^r
HopAF1	pCPP5539	Kan^r
HopAM1	pCPP5052	Kan^r
HopAO1	pCPP5537	Kan^r
HopAD1	pCPP6450	Kan^r

***** construct includes chaperone

784

Table S4 Primers utilized in this study. All primers were designed specifically for this project 765

Primer target	Direction	Sequence
pCPP5372 pre attR1 site	Fw	CCCTATGACCACTCAAGTGGCG
M13	Fw	CGACGTTGTAAAACGACGGCCAG
5912_Rv	Rev	CTTGGGTGCGCTATGGGTAT
5154_Rv	Rev	CACCCTTTTGCCAGTTACGG
5530_Rv	Rev	AGGCATCGCTGATCACTTCC
5617_Rv	Rev	TCATCGATCACCAGACTGCG
5053_Rv	Rev	GGAGCCCTTCACCATGACAA
5588_Rv	Rev	TTGGACGTGATCTTGGGAGC
5618_Rv	Rev	GGGTCTTGAAGTCCAGCTCC
5058_Rv	Rev	GTAACAGACCCTTTCGACCGG
5238_Rv	Rev	TTTCGCGGAGAGAATGCCTT
5306_Rv	Rev	CGGATGGAGTTCTCTGACGG
5571_Rv	Rev	TCAGGGTGGTTCTTCATCGC
5099_Rv	Rev	CCTTGCAGTAGAGCGTGTCG
5233_Rv	Rev	CAGTTGATCAGCGACCGACT
5060_Rv	Rev	GTATCGCAAGTGAAAGTCTGCTC
5910_Rv	Rev	ACCGCTATTCATTGCCTCGA
MM0038_3373_Rv	Rev	GCGCCCACCCTTATCTGG
MM0039_5951_Rv	Rev	ATGAACAGTGTCGTCTCGGG
MM0040_3416_Rv	Rev	CGCGCCCACCCTTTGAC
MM0041_5328_Rv	Rev	CGCCCACCCTTAATCTGACT
MM0042_5741_Rv	Rev	CCGGATGGCTCTCGAAATGA
MM0043_5534_Rv	Rev	TTTGATGGGCGAGACTTGCT
MM0044_3417_Rv	Rev	CCACCCTTCTGGTAGTTGATGC
MM0045_5107_Rv	Rev	GGATGCAGTCGATTTCACCG
MM0046_5108_Rv	Rev	TCACTTCGAGAAAACGCCGA
MM0047_5616_Rv	Rev	ACATGTCTTTCAAGGGCCGT
MM0048_5539_Rv	Rev	ACCCTTTTGTGCGACCAGAT
MM0049_5052_Rv	Rev	GGTGTGCTTGCCATCATGAC
MM0050_5537_Rv	Rev	TAGTCGTGAAAGGCCTGCAG
MM0051_6450_Rv	Rev	CCCGTGAGTCTTGTCCTAGC

Table S5: Elicitors tested for ROS burst elicitation on spinach.

Elicitor-candidate	Description	Concen-tration	Producer/ Source	Reference (if applicable)
Chitin	Cell wall component of fungi, recognised by different receptors depending on the plant	4 mg mL^{-1}	Merck C7170, from shrimp shells, processing described in (Johanndrees et al., 2022)	(Sánchez-Vallet et al., 2015)
flg22	22 amino acid peptide of *Pseudomonas aeruginosa* flagellin	0.2 µM	Synthesised by Genscript; RP19986	(Mersmann et al., 2010)
nlp24	24 amino acid peptide of *Hyaloperonospora arabidopsidis* of the necrosis and ethylene-inducing peptide 1-like protein 3 (HaNLP3)	2 µM	Synthesised by Genscript	(Oome et al., 2014)
***P. effusa 1* sporangia**	Heat-lysed *P. effusa* race 1 sporangia	150 sporangia/µL	Sporangia harvested 14 dpi, cleaned with a vacuum filtration system combining Miracloth, spore collection on a 11 µm Merck Millipore Nylon net filter (NY1104700)	(Klein et al., 2020; Skiadas et al., 2022)
MAMP-mix	Heat-lysed D36E	OD_{600} equal to 1.0	Grown as described above, dilution/re-suspension in MQ	(Wei et al., 2015)

786